



**HAL**  
open science

# Hydromechanical field theory of plant morphogenesis

Hadrien Oliveri, Ibrahim Cheddadi

► **To cite this version:**

Hadrien Oliveri, Ibrahim Cheddadi. Hydromechanical field theory of plant morphogenesis. 2024.  
hal-04867942

**HAL Id: hal-04867942**

**<https://inria.hal.science/hal-04867942v1>**

Preprint submitted on 6 Jan 2025

**HAL** is a multi-disciplinary open access archive for the deposit and dissemination of scientific research documents, whether they are published or not. The documents may come from teaching and research institutions in France or abroad, or from public or private research centers.

L'archive ouverte pluridisciplinaire **HAL**, est destinée au dépôt et à la diffusion de documents scientifiques de niveau recherche, publiés ou non, émanant des établissements d'enseignement et de recherche français ou étrangers, des laboratoires publics ou privés.



Distributed under a Creative Commons Attribution 4.0 International License

# Hydromechanical field theory of plant morphogenesis

Hadrien Oliveri<sup>a,b,c,\*</sup>, Ibrahim Cheddadi<sup>d,e,\*\*</sup>

<sup>a</sup>Max Planck Institute for Plant Breeding Research, Cologne, 50829, Germany

<sup>b</sup>Max Planck Institute of Molecular Cell Biology and Genetics, Dresden, 01307, Germany

<sup>c</sup>Center for Systems Biology Dresden, Dresden, 01307, Germany

<sup>d</sup>Université Grenoble Alpes, CNRS, Grenoble INP, TIMC, Grenoble, 38000, France

<sup>e</sup>Laboratoire de Reproduction et Développement des Plantes, Université de Lyon, ENS de Lyon, UCBL, INRAE, CNRS, Inria, Lyon, 69364, France

---

## Abstract

The growth of plants is a hydromechanical phenomenon in which cells enlarge by absorbing water, while their walls expand and remodel under turgor-induced tension. In multicellular tissues, where cells are mechanically interconnected, morphogenesis results from the combined effect of local cell growths, which reflects the action of heterogeneous mechanical, physical, and chemical fields, each exerting varying degrees of nonlocal influence within the tissue. To describe this process, we propose a physical field theory of plant growth. This theory treats the tissue as a *poromorphoelastic* body, namely a growing poroelastic medium, where growth arises from pressure-induced deformations and osmotically-driven imbibition of the tissue. From this perspective, growing regions correspond to hydraulic sinks, leading to the possibility of complex non-local regulations, such as water competition and growth-induced water potential gradients. More in general, this work aims to establish foundations for a mechanistic, mechanical field theory of morphogenesis in plants, where growth arises from the interplay of multiple physical fields, and where biochemical regulations are integrated through specific physical parameters.

**Keywords:** plant mechanics, morphogenesis, growth, elasticity, morphoelasticity, poroelasticity  
**2020 MSC:** 74B20, 74F10, 74F20, 92B99

---

*Einfach schlief in dem Samen die Kraft; ein beginnendes Vorbild  
Lag, verschlossen in sich, unter die Hülle gebeugt,  
Blatt und Wurzel und Keim, nur halb geformt und farblos;  
Trocken erhält so der Kern ruhiges Leben bewahrt,  
Quillet strebend empor, sich milder Feuchte vertrauend,  
Und erhebt sich sogleich aus der umgebenden Nacht.*

---

Johann Wolfgang von Goethe, *Die Metamorphose der Pflanzen*, 1798

---

\*holiveri@mpipz.mpg.de

\*\*ibrahim.cheddadi@univ-grenoble-alpes.fr

# 1. Introduction

## 1.1. Modelling the growth of plant tissues

Morphogenesis is the fundamental process by which biological organisms establish their shape. This phenomenon relies upon multiple genetic, chemical, mechanical, and physical regulations, which are typically multiscale, thermodynamically open, out-of-equilibrium, and coupled in a so-called complex system. To achieve a rational understanding of morphogenesis, dedicated models are indispensable; in particular, a grand challenge is to build mechanistic continuum theories that describe the emergent physical behaviour of living tissues at the macroscopic scale.

In plants, the key phenomenon driving morphogenesis is *growth*, the general process by which a physical body deforms by gaining mass (Goriely, 2017). Indeed, in plant tissues, adjoining cells are mechanically interconnected and constrained by an extracellular cell wall matrix which prevents cell migration and topological rearrangements (Boudaoud, 2010; Coen and Cosgrove, 2023; Hamant and Traas, 2010). Therefore, complex organ shapes result from the anisotropic and heterogeneous growth (and division) of the cells, generating large solid deformations of connected tissue regions (Boudaoud, 2010; Coen et al., 2004).

The theory of *morphoelasticity* is a modern mechanical theory of growth, which has emerged historically from the nonlinear field theories of elasticity and elastoplasticity (Goriely, 2017). This framework has been adapted with remarkable success to a wealth of biological systems (see the reviews by Ambrosi et al., 2019; Kuhl, 2014; Menzel and Kuhl, 2012), and provides a natural framework to model plant growth at the tissue scale (Boudaoud et al., 2023; Dervaux and Ben Amar, 2008; Goriely et al., 2010; Holland et al., 2013; Liang and Mahadevan, 2009; Moulton et al., 2020; Oliveri et al., 2024; Vandiver and Goriely, 2008). Historically, an important problem in growth theory has been the characterisation of growth-induced mechanical instabilities, which refer to the loss of stability and change in configuration undergone by a growing tissue as a result to growth-induced internal stresses (e.g. Ben Amar and Goriely, 2005; Dervaux and Ben Amar, 2008; Goriely and Tabor, 1998; Jia et al., 2018; Liang and Mahadevan, 2009; Liu et al., 2013; Wang and Zhao, 2015). In this context, the growth deformation is treated typically as a constant bifurcation parameter controlling the onset of instability. In this respect, the focus lies on the static elasticity problems arising from growth, rather than the physical origin and kinetics of growth itself. In contrast, the so-called problem of *morphodynamics* consists in studying growth as a variable of a dynamical system whose evolution reflects the physical state of the tissue, reflecting the inherently dynamic nature of developmental processes (Chickarmane et al., 2010; Vandiver and Goriely, 2009).

From a biological point of view, plant growth is controlled dynamically through a multitude of genes and hormones that form heterogeneous patterning fields (Coen, 1999; Johnson and Lenhard, 2011). To address the role of genetic patterning in morphogenesis, continuum computational models have been proposed, based on the so-called notion of *specified growth*, detailed in Coen et al. (2004); Kennaway and Coen (2019); Kennaway et al. (2011) and applied in various context, see Green et al. (2010); Kelly-Bellow et al. (2023); Kierzkowski et al. (2019); Lee et al. (2019); Peng et al. (2022); Rebocho et al. (2017); Whitewoods and Coen (2017); Whitewoods et al. (2020); Zhang et al. (2024, 2020) (see also Ali et al., 2014; Coen and Cosgrove, 2023; Coen et al., 2017; Mosca et al., 2018, for reviews). Specified growth refers to the *intrinsic* growth a volume element undergoes when isolated from the rest of the tissue, reflecting some local biological identity (e.g.

gene expression, polarity or, more abstractly, the action of morphogens) which control the kinematics of growth. Then, given a specified growth field, a compatible deformation can be obtained in a second step, by minimising the body’s elastic energy. This approach has been instrumental in demonstrating how spatially heterogeneous gene expression patterns control the emergence of complex shapes in three-dimensions. However, from a biophysical perspective, specified growth remains a fundamentally phenomenological and essentially kinematic representation of growth, as its precise link to cellular mechanics—specifically the explicit physical action of genes—is not fully characterised.

In contrast, the aim of biophysics is to explain growth from physical and mechanical principles. In this context, physically-based discrete models describe tissues at the cellular level, incorporating detailed cellular structure and geometry, mechanical anisotropies, and fine mechanisms underlying growth (Ali et al., 2019; Alim et al., 2012; Bassel et al., 2014; Bessonov et al., 2013; Bou Daher et al., 2018; Boudon et al., 2015; Cheddadi et al., 2019; Corson et al., 2009; Dupuy et al., 2007; Fozard et al., 2013; Fridman et al., 2021; Hamant et al., 2008; Kelly-Bellow et al., 2023; Khadka et al., 2019; Liu et al., 2022; Long et al., 2020; Merks et al., 2011; Peng et al., 2022; Rudge and Haseloff, 2005; Sassi et al., 2014; Zhao et al., 2020). The goal in these models is then to reproduce the growth phenomenon from first principles, thereby allowing for rigorous testing of hypotheses at the cellular scale through specific biophysical parameters. However, this type of approach relies on a discretised representation of the tissue, thus it is often doomed to remain computational. While cellular models offer detailed insights, they do not enjoy the generality, minimalism, scalability, and analytic tractability of a continuum mathematical theory.

### 1.2. *The hydromechanical basis of cell growth*

To build such a theory on physical grounds, we start with the basic physics of cell expansion. Plant cells grow by absorbing water from their surrounding—a process driven by their relatively high osmolarity (Geitmann and Ortega, 2009; Ortega, 2010; Schopfer, 2006). This phenomenon is captured by the historical model of Lockhart (1965), later expanded in a somewhat similar manner by Cosgrove (1981, 1985) and Ortega (1985) (see also the discussions by Ali et al., 2023; Cheddadi et al., 2019; Dumais, 2021; Forterre, 2013, 2022; Geitmann and Ortega, 2009; Goriely et al., 2008a; Ortega, 2010). This model describes the elongation of a single cylindrical cell of length  $\ell$ . The expansion rate  $\dot{\ell}$  of such cell can be expressed in terms of the volumetric influx of water through (Dainty, 1963)

$$\dot{\ell} = k_c \ell (\pi - p), \quad (1)$$

with  $k_c$  the effective hydraulic conductivity the cell;  $\pi$  and  $p$  respectively the excess osmotic and hydrostatic pressures with respect to the outside; and where the overdot denotes differentiation w.r.t. time  $t$ . The quantity  $\psi = p - \pi$ , the *water potential* of the cell relative to the outside, characterises the capacity of the cell to attract water. Note that (1) does not define a closed system, as the pressure  $p$  is related to the mechanics of the cell wall via the balance of forces. The growth of plant cells is a complex process that involves loosening, yielding under tension, and remodelling of the cell walls (Cosgrove, 2005, 2016, 2018). This process is modelled as a Maxwell-type viscoelastoplastic creep. In an elongating cylindrical cell, stress can be explicitly written in terms of



pressure, and this rheological law can be written as

$$\frac{\dot{\ell}}{\ell} = \Phi(p - y)_+ + \frac{\dot{p}}{E}, \quad (2)$$

with  $(x)_+ := \max(x, \cdot)$  the ramp function;  $y$  a threshold pressure above which growth occurs;  $\Phi$  the so-called *extensibility* of the cell; and  $E$  the effective Young's modulus of the cell. Equations (1, 2) now form a closed system for  $\ell$  and  $p$ , illustrating that the turgor pressure is not a control parameter of the rate of growth, but a dependent variable of the cell expansion process. Indeed, in the steady growth regime ( $\dot{p} = 0$ ), the pressure is fully determined by the three parameters  $y$ ,  $\pi$  and  $\alpha_c := k_c/(k_c + \Phi)$ , and can be eliminated from the system:

$$\frac{\dot{\ell}}{\ell} = \alpha_c \Phi(\pi - y), \quad p = \alpha_c \pi + (1 - \alpha_c)y \quad (3)$$

(with  $y \leq p \leq \pi$ ).

Recently, the Lockhart model served as a starting point for a vertex-based, multicellular hydromechanical model of plant morphogenesis, including water movements between cells, and mechanically-driven cell wall expansion (Cheddadi et al., 2019). This generalisation of the single-cell model generates several additional emergent spatiotemporal effects that arise from the coupling between wall expansion and water movements within a large developing tissue, such as hydraulic competition effects and water gradients. Overall, the relationship between water and growth, as highlighted by the Lockhart-Ortega-Cosgrove model and its multidimensional generalisation, is central to the physical functioning of plant living matter, and the basic notion that water must travel from sources (e.g. vasculature) to growing regions is a fundamental principle of development.

### 1.3. Hydromechanical field theory for plant growth

Building on this notion, we here develop a physical field theory of plant morphogenesis including tissue mechanics, wall synthesis, and hydraulics. Viewing the tissue as a network of cells exchanging water, a natural formalism is the theory of porous media, which describes the deformations of fluid-saturated materials. The modern theory of porous media has a complex history originating in the seminal works of Fick and Darcy on diffusion, and Fillunger, Terzaghi and Biot on soil consolidation, formalised later within the context of the theory of mixtures, notably based on contributions by Truesdell and Bowen (Bedford and Drumheller, 1983; De Boer, 1992, 2012). There is now a rich body of literature exploring the application of these concepts to biology in various contexts, including biological growth. However, despite the clear significance of water in plant mechanics (Dumais and Forterre, 2012; Forterre, 2022), the role of hydromechanics in the context of plant growth modelling has but marginally been examined. Several notable works have featured linear poroelastic descriptions of plant matter, occasionally including growth (Molz and Boyer, 1978; Molz and Ikenberry, 1974; Molz et al., 1975; Passioura and Boyer, 2003; Philip, 1958; Plant, 1982); however, these studies are limited to simple geometries and have not culminated in a general three-dimensional theory of growth. While the limiting role of water fluxes within plant tissues has long been debated (Boyer, 1988; Cosgrove, 1993) and remains challenging to assess experimentally, recent years have seen a resurgence of interest in this problem, with new

studies supporting the potential for hydromechanical control in tissue development (Alonso-Serra et al., 2024; Cheddadi et al., 2019; Laplaud et al., 2024; Long et al., 2020). Building on these recent advancements, we propose a hydromechanical model for plant tissues seen as morphoelastic, porous materials encompassing the solid matrix of the cells and their fluid content. Technically speaking, our approach is analogous to previous models, for instance for tumour growth (Fraldi and Carotenuto, 2018; Xue et al., 2016) or brain oedema (Lang et al., 2015), however the specificities of plant living matter demand a dedicated treatment. Overall, this work aims to bridge the conceptual gap between cell biophysics and growth at the tissue scale, by describing growth as a consequence of simultaneous mechanical deformations and imbibition of the cells, thereby extending the seminal analysis of Lockhart to the framework of continuum media.

The goals are then (i) to establish theoretical foundations for a generic theory of plant growth within the framework of nonlinear continuum mechanics (Section 2); and (ii) to characterise the guiding principles that emerge from multiple couplings between mechanical, physical and hydraulic fields (Sections 3–5).

## 2. General theory

### 2.1. Geometry and kinematics

#### 2.1.1. Total deformation

We describe the geometry and kinematics of the evolving tissue viewed as a continuum domain embedded in the three-dimensional space (see Goriely, 2017; Holzapfel, 2000, for details on finite strain theory). We introduce the initial configuration  $\mathcal{B}_0 \subset \mathbb{R}^3$  at time  $t = 0$  of the body, and its current configuration  $\mathcal{B} \subset \mathbb{R}^3$  at  $t \geq 0$ ; see Fig. 1(a). The deformation of the body from  $\mathcal{B}_0$  to  $\mathcal{B}$  is described by a smooth map  $\chi : \mathcal{B}_0 \times \mathbb{R} \rightarrow \mathcal{B}$  that sends material points  $\mathbf{X} \in \mathcal{B}_0$  onto spatial points  $\mathbf{x} = \chi(\mathbf{X}, t) \in \mathcal{B}$ , at a given time  $t \in \mathbb{R}$ . The deformation gradient tensor is defined as  $\mathbf{F} := \text{Grad} \chi$ , with Grad the material (or Lagrangian) gradient, with respect to the reference configuration. Finally, the Jacobian determinant of the deformation,  $J := \det \mathbf{F}$ , measures the local volumetric expansion due to  $\chi$  (i.e.  $dv = JdV$ ).

Next, we describe the kinematics of the deformation by introducing the material and spatial (or Eulerian) velocities, respectively  $\mathbf{V}$  and  $\mathbf{v}$ , defined as  $\mathbf{V}(\mathbf{X}, t) = \mathbf{v}(\mathbf{x}, t) = \partial \chi(\mathbf{X}, t) / \partial t$ . A natural measure of the relative rate of deformation is then the gradient of spatial velocity,

$$\mathbf{L} := \text{grad} \mathbf{v} = \dot{\mathbf{F}} \mathbf{F}^{-1}, \quad (4)$$

with  $\text{grad}(\cdot) = \mathbf{F}^{-\top} \text{Grad}(\cdot)$  the Eulerian gradient with respect to the current configuration. We also recall the standard kinematic formulae  $\dot{J}/J = \text{div} \mathbf{v} = \text{tr} \mathbf{L}$ , with div the Eulerian divergence and tr the trace operator. Here, the overdot denotes the material derivative  $\dot{J} = dJ/dt$ , related to the Eulerian derivative  $\partial J / \partial t$  through the generic formula

$$\dot{J} = \frac{\partial J}{\partial t} + \mathbf{v} \cdot \text{grad} J. \quad (5)$$

### 2.1.2. Growth

We model growth using the framework of morphoelasticity (Goriely, 2017). The fundamental postulate of morphoelasticity is the multiplicative decomposition of deformations into an elastic deformation tensor  $\mathbf{A}$  and a growth tensor  $\mathbf{G}$  (Rodriguez et al., 1994):

$$\mathbf{F} = \mathbf{A}\mathbf{G}; \quad (6)$$

see Fig. 1(a). Constitutively, the growth deformation  $\mathbf{G}$  is assumed to be *anelastic*, meaning it does not contribute to the strain energy, and describes the configurational change in the local reference configuration of the body due to local mass addition. In contrast, the elastic deformation  $\mathbf{A}$  generates stresses and enters the strain energy function. Note that there is no requirement for the growth deformation to be compatible, that is, in general there is no deformation embeddable in the Euclidean space of which  $\mathbf{G}$  is the gradient, unlike  $\mathbf{F}$  which is compatible by definition (see Goriely, 2017, Chapter 12). We define the Jacobian determinants  $J_A := \det \mathbf{A}$  and  $J_G := \det \mathbf{G}$ , so that (6)

$$J = J_A J_G; \quad (7)$$

and the rate of growth  $\mathbf{L}_G := \dot{\mathbf{G}}\mathbf{G}^{-1}$  and rate of elastic deformation  $\mathbf{L}_A := \dot{\mathbf{A}}\mathbf{A}^{-1}$ , with

$$\mathbf{L} = \mathbf{L}_A + \mathbf{A}\mathbf{L}_G\mathbf{A}^{-1}. \quad (8)$$

Finally, we introduce  $\Gamma := \text{tr } \mathbf{L}_G = \dot{J}_G/J_G$ , measuring the relative rate of volumetric expansion due to growth.

Note that, in the context of plant morphogenesis, most authors have restricted their attention to linear elasticity. In contrast, as we do not require  $\mathbf{A}$  or  $\mathbf{G}$  to be small here, our approach is geometrically exact and can capture arbitrarily large strains, and rich elastic behaviours such as strain-stiffening effects (Kierzkowski et al., 2012).

## 2.2. Balance laws

### 2.2.1. Balance of mass

We model the growing tissue as a *poromorphoelastic* solid representing the cell matrices and the water content; see Fig. 1(b). Specifically, the tissue is viewed as a triphasic porous medium composed of a solid phase representing the extracellular cell wall matrix ('s'), a pure fluid phase ('f'), and the cytoplasmic osmolytes ('o'). We define  $\mathbf{v}_s$ ,  $\mathbf{v}_f$ , and  $\mathbf{v}_o$ , the Eulerian velocities of the respective phases, with the solid velocity chosen as the reference:

$$\mathbf{v}_s = \mathbf{v}. \quad (9)$$

We denote with  $\phi_s$ ,  $\phi_f$ ,  $\phi_o$  the volume fractions of the solid, fluid and osmolyte components, respectively, in the current configuration (that is, the true volume occupied by each component per unit volume of tissue). Assuming that the material is saturated, we have

$$\phi_s + \phi_f + \phi_o = 1. \quad (10)$$

The pore space volume occupancy is measured by the Eulerian porosity  $\phi := 1 - \phi_s$ , which represents the ratio of pore space volume to current tissue volume. Similarly, the intermediate porosity

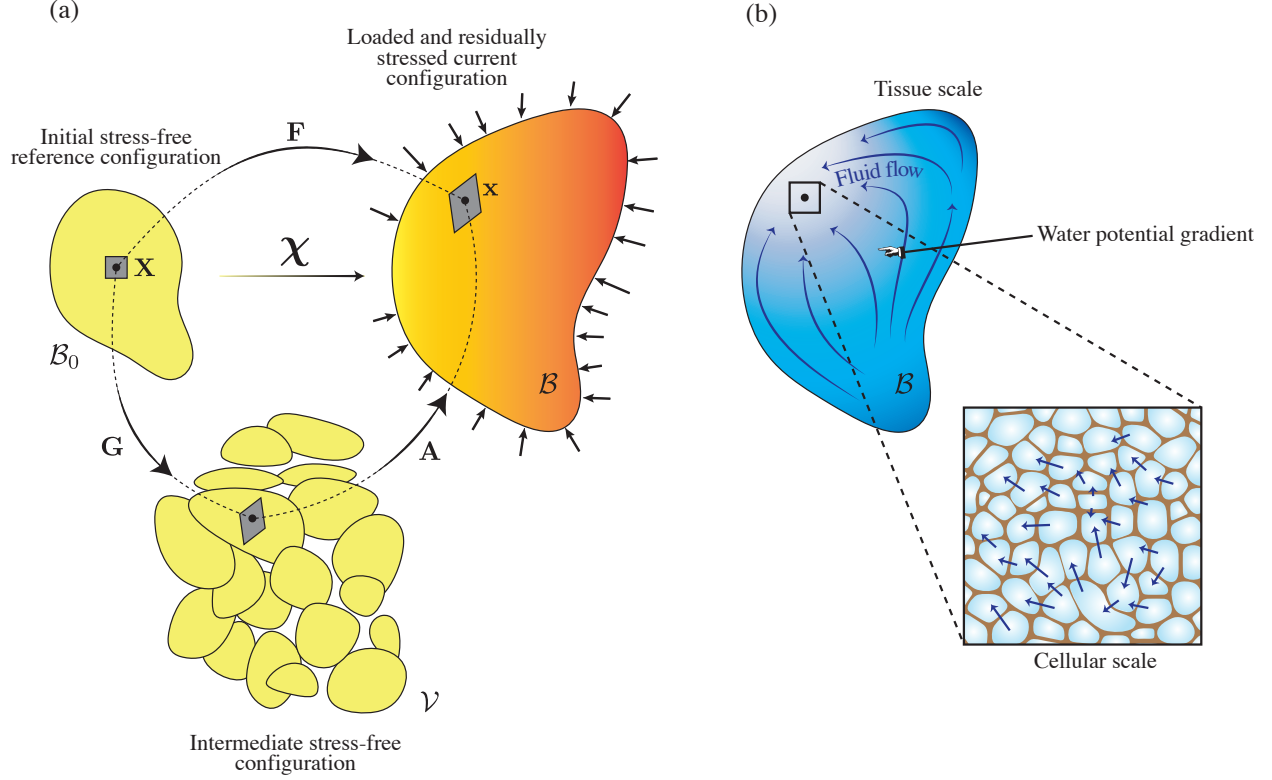


Figure 1: Poromorphoelastic theory of plant morphogenesis. (a) The multiplicative decomposition of morphoelasticity (redrawn after [Goriely, 2017](#)). Starting from a stress-free initial configuration, a local growth deformation  $\mathbf{G}$  is applied on volume elements, resulting in an incompatible intermediate configuration. A second deformation  $\mathbf{A}$  allows to ensure compatibility, and results in a stressed configuration that is loaded externally and includes residual growth stresses. (b) The material is modelled as a growing porous medium, capturing the flow of water across the domain.

$\Phi := J_A \phi$  measures the *current* pore space volume per unit *intermediate* volume. The Lagrangian porosity  $\Phi^0 := J\phi = J_G \Phi$  measures the current pore space volume per unit reference volume.

Here, we assume that all phases are *inherently* elastically incompressible ([Lang et al., 2015](#)). This assumption implies that in a macroscopic elastic deformation, the pores will shrink or dilate so as to conserve the volume of the solid phase. Thus, we can relate the solid volume fraction in the unstressed configuration ( $\Phi_s$ , the solid volume fraction observed upon relieving the stresses) to that in the current configuration  $\phi_s$ , through

$$\Phi_s = J_A \phi_s = J_A - \Phi. \quad (11)$$

During growth and remodelling of the tissue, cells secrete new solid material, divide and form new cell walls that may affect the structure of the cell matrix locally, thus, the porosity. To represent this effect, we assume generally that the solid volume fraction may evolve as

$$\dot{\Phi}_s = \mathcal{H}(\mathbf{x}, t, \Phi_s, \mathbf{G}, \dots), \quad (12)$$

where  $\mathcal{H}$  is a function of the different variables that symbolises the local evolution of the matrix structure during growth. For example, in a scenario where cells do not divide but maintain a constant cell wall thickness, we can assume  $\mathcal{H} = -\Gamma \Phi_s / 3$ . We assume here that the tissue maintains

locally a constant homeostatic cellular structure, so that  $\mathcal{H} = 0$  and  $\Phi_s$  is a constant. We can rewrite (12) using (5, 7, 11) as

$$\frac{\partial \phi_s}{\partial t} + \operatorname{div}(\phi_s \mathbf{v}_s) = \mathcal{H}/J_G + \Gamma \phi_s := \xi_s, \quad (13)$$

with  $\xi_s$  representing the source of solid material. Here we assume that the availability of the solid material required for growth is non-limiting, i.e., we ignore the physiological aspects of biosynthesis underlying growth (photosynthesis, nutrient uptake).

Similarly, the balance of fluid mass is expressed through

$$\frac{\partial \phi_f}{\partial t} + \operatorname{div}(\phi_f \mathbf{v}_f) = \xi_f, \quad (14)$$

where  $\xi_f$  is a possible source of water that accounts, typically, for a bulk vascularisation of the tissue. A possible constitutive law for  $\xi_f$  is discussed later in this paper. Lastly, the balance of mass for the osmolytes is expressed through

$$\frac{\partial \phi_o}{\partial t} + \operatorname{div}(\phi_o \mathbf{v}_o) = \xi_o. \quad (15)$$

with  $\xi_o$  representing the synthesis/uptake of osmolytes. Summing (13–15) using (9, 10), we obtain a single volume balance equality (Lang et al., 2015):

$$\operatorname{div}(\phi_s \mathbf{v} + \phi_f \mathbf{v}_s + \phi_o \mathbf{v}_o) = \xi_s + \xi_f + \xi_o. \quad (16)$$

### 2.2.2. Balance of momentum

Since the growth and fluid transport happen at timescales (hours) that are much longer than the timescale of elastic relaxation (seconds), we neglect inertia. Thus, we write the balance of momentum in terms of the Cauchy stress tensor  $\mathbf{T}$  as

$$\operatorname{div} \mathbf{T} + \mathbf{b} = \mathbf{0}, \quad \mathbf{T} = \mathbf{T}^\top, \quad (17)$$

with  $\mathbf{b}$  a density of applied body loads (per unit current volume), typically self-weight in our context. Henceforth, we focus on the case  $\mathbf{b} = \mathbf{0}$ . The symmetry of the stress tensor results from the absence of applied torque and micropolar structure in the material. In a more general theory, asymmetric stresses may be introduced to reflect the possible local twist of the cells (Chakraborty et al., 2021; Wada, 2012).

### 2.2.3. Balance of internal energy

To complete the theory, we discuss the thermodynamics of the system. The balance of energy for the total internal energy  $\mathcal{E}$  of a region  $\Omega \subset \mathcal{B}$  encompasses internal work contributions  $\mathcal{P}$ , heat  $\mathcal{Q}$ , and addition of new material  $\mathcal{S}$ :

$$\frac{d\mathcal{E}}{dt} = \mathcal{P} + \mathcal{Q} + \mathcal{S}, \quad (18)$$

where

$$\mathcal{E} = \int_{\Omega} e \, dv, \quad (19)$$

with  $e$  the internal energy per unit volume of mixture. The work rate encompasses the work of internal forces, the works required to make room for new fluid, osmolyte and solid material ( $w_s$ ) during growth, and the work  $\bar{w}_o$  accounting for the active transport of the osmolytes, reflecting chemical processes that we do not address explicitly. Altogether, we have

$$\mathcal{P} = \int_{\Omega} \mathbf{T} : \mathbf{L} \, dv + \int_{\Omega} p \xi_f \, dv - \int_{\partial\Omega} p \mathbf{j}_f \cdot \mathbf{da} + \int_{\Omega} p \xi_o \, dv - \int_{\partial\Omega} p \mathbf{j}_o \cdot \mathbf{da} + \int_{\Omega} w_s \xi_s \, dv + \int_{\Omega} \bar{w}_o \, dv, \quad (20)$$

where  $\mathbf{j}_f = \phi_f \mathbf{w}_f$  and  $\mathbf{j}_o = \phi_o \mathbf{w}_o$  are the relative fluxes of fluid and osmolytes through the mixture; with  $\mathbf{w}_f := \mathbf{v}_f - \mathbf{v}$  the seepage velocity of the fluid and  $\mathbf{w}_o := \mathbf{v}_o - \mathbf{v}$ ; and where  $\mathbf{da}$  and  $dv$  denote respectively the outward normal surface element and the volume element for the integration. The heat contribution encompasses a bulk source  $r$  and a flux  $\mathbf{q}$  through the boundary:

$$\mathcal{Q} = \int_{\Omega} r \, dv - \int_{\partial\Omega} \mathbf{q} \cdot \mathbf{da}. \quad (21)$$

Energy is also added to the system through addition of new material. We note  $e_f$ ,  $e_o$  and  $e_s$  the internal energy of the fluid, the osmolytes and the solid so that

$$\mathcal{S} = \int_{\Omega} e_s \xi_s \, dv + \int_{\Omega} e_f \xi_f \, dv - \int_{\partial\Omega} e_f \mathbf{j}_f \cdot \mathbf{da} + \int_{\Omega} e_o \xi_o \, dv - \int_{\partial\Omega} e_o \mathbf{j}_o \cdot \mathbf{da}. \quad (22)$$

Using the divergence theorem to eliminate the boundary terms, then the Leibniz rule for differentiation under the integral sign, and the localisation theorem, we derive the local form of the balance of internal energy

$$\frac{\partial e}{\partial t} + \operatorname{div}(e\mathbf{v}) = \mathbf{T} : \mathbf{L} + r + h_f \xi_f + h_o \xi_o + h_s \xi_s + \bar{w}_o - \operatorname{div}(h_f \mathbf{j}_f + h_o \mathbf{j}_o + \mathbf{q}), \quad (23)$$

where we have introduced  $h_f = e_f + p$ ,  $h_o = e_o + p$  and  $h_s = e_s + w_s$  the enthalpies per unit volume of pure fluid, osmolytes and solid material, respectively. Alternatively, it is convenient to express the balance of energy in reference configuration as

$$\dot{E}^0 = \mathbf{P} : \dot{\mathbf{F}} + R^0 + h_f \Xi_f^0 + h_o \Xi_o^0 + h_s \Xi_s^0 + \bar{W}_o^0 - \operatorname{Div}(h_f \mathbf{J}_f^0 + h_o \mathbf{J}_o^0 + \mathbf{Q}^0), \quad (24)$$

where  $\operatorname{Div}$  denotes the Lagrangian divergence;  $E^0 = J e$  is the internal energy per unit reference volume;  $\mathbf{P} = J \mathbf{T} \mathbf{F}^{-\top}$  is the Piola–Kirchhoff stress (Holzapfel, 2000); and  $\mathbf{Q}^0 = J \mathbf{F}^{-1} \mathbf{q}$ ,  $\mathbf{J}_o^0 = J \mathbf{F}^{-1} \mathbf{j}_o$  and  $\mathbf{J}_f^0 = J \mathbf{F}^{-1} \mathbf{j}_f$  are the flux terms pulled back to the reference configuration. We define the quantities  $\Phi_f^0 = J \phi_f$ ,  $\Phi_o^0 = J \phi_o$ , and  $\Phi_s^0 = J \phi_s = J_G \Phi_s$ , measuring respectively the current volume of each component per unit reference volume, so that  $\Xi_s^0 = \Phi_s^0 \Gamma$ ,  $\Xi_o^0 = J \xi_o$  and  $\Xi_f^0 = J \xi_f$  are the local production of solid, osmolytes and fluid volume per unit reference volume;  $R^0 = J r$  is the heat source per unit reference volume;  $\bar{W}_o^0 = J \bar{w}_o$  is the work due to active transport per unit reference volume.

#### 2.2.4. Imbalance of entropy

The second law of thermodynamics is expressed through the Clausius-Duhem inequality, expressed in terms of the entropy density  $S^0$  (entropy per unit initial volume) as (Goriely, 2017; Xue et al., 2016)

$$\dot{S}^0 \geq \frac{R^0}{\theta} + s_f \Xi_f^0 + s_o \Xi_o^0 + s_s \Xi_s^0 + \bar{S}_o^0 - \text{Div} \left( \frac{\mathbf{Q}^0}{\theta} + s_f \mathbf{J}_f^0 + s_o \mathbf{J}_o^0 \right), \quad (25)$$

with  $\theta$  denoting the thermodynamic temperature; and where  $s_f$ ,  $s_o$  and  $s_s$  are the volumetric entropy densities of the added fluid, osmolyte and solid materials, respectively; and  $\bar{S}_o^0$  denotes the entropy contribution from active transport. Henceforth, we assume isothermal conditions for simplicity, so we take  $\mathbf{Q}^0 = \mathbf{0}$  and  $R^0 = 0$ . Introducing the Helmholtz free energy  $\Psi^0 = E^0 - \theta S^0$  and applying the energy balance equation (24), we can reformulate the previous inequality as

$$\dot{\Psi}^0 \leq \mathbf{P} : \dot{\mathbf{F}} + g_f \Xi_f^0 + g_o \Xi_o^0 + g_s \Xi_s^0 + \bar{G}_o^0 - \text{Div} (g_f \mathbf{J}_f^0 + g_o \mathbf{J}_o^0), \quad (26)$$

where  $g_s = h_s - \theta s_s$ ,  $g_f = h_f - \theta s_f$  and  $g_o = h_o - \theta s_o$  denote the Gibbs free energy densities of the solid, fluid and solute material, respectively; and  $\bar{G}_o^0 := \bar{W}_o^0 - \theta \bar{S}_o^0$ . As detailed in the next section, the inequality (26) is useful to derive constitutive laws for growth and material transport.

### 2.3. Constitutive laws

#### 2.3.1. Coleman-Noll procedure

To close the system we need to formulate constitutive laws for the material. Therefore, we follow the approach of Xue et al. (2016) and apply the Coleman-Noll procedure to the dissipation inequality (26) to constrain thermodynamically the constitutive laws (Coleman and Noll, 1963; Goriely, 2017; Gurtin et al., 2010). Firstly, we decompose the free energy  $\Psi^0$  into a solid part  $\Psi_s^0$  and a fluid part  $\Psi_f^0 = \Phi_f^0 g_f + \Phi_o^0 g_o - \Phi^0 p$  (Coussy, 2003); so that  $\Psi^0 = \Psi_s^0 + \Phi_f^0 g_f + \Phi_o^0 g_o - \Phi^0 p$ . For an inherently incompressible solid component, the porosity  $\Phi^0 = J_G(J_A - \Phi_s)$  is determined by the deformation. We introduce the mechanical free energy of the material in the form

$$W^0(\mathbf{A}, \mathbf{G}, p) = \Psi_s^0(\mathbf{A}, \mathbf{G}) - p J_G(J_A - \Phi_s), \quad (27)$$

encompassing an elastic contribution and a hydrostatic contribution. The energy per unit intermediate volume is

$$W(\mathbf{A}, p) = J_G^{-1} W^0(\mathbf{A}, \mathbf{G}, p) = \Psi_s(\mathbf{A}) - p(J_A - \Phi_s), \quad (28)$$

where  $\Psi_s(\mathbf{A}) = J_G^{-1} \Psi_s^0(\mathbf{A}, \mathbf{G})$  defines the strain energy density of the solid, per unit intermediate volume. Then, combining (26, 27) with the balance of mass relations  $\dot{\Phi}_f^0 = \Xi_f^0 - \text{Div} \mathbf{J}_f^0$  and  $\dot{\Phi}_o^0 = \Xi_o^0 - \text{Div} \mathbf{J}_o^0$  (14, 15), and the Gibbs-Duhem equality  $\dot{p} \Phi^0 = \dot{g}_f \Phi_f^0 + \dot{g}_o \Phi_o^0$ , we obtain

$$\dot{W}^0 \leq \mathbf{P} : \dot{\mathbf{F}} - \dot{p} \Phi_f^0 + \bar{G}_o^0 - \mathbf{J}_f^0 \cdot \text{Grad} g_f - \mathbf{J}_o^0 \cdot \text{Grad} g_o. \quad (29)$$

Finally, expanding  $\dot{W}^0$  as  $\dot{W}_0 J_G^{-1} = \mathbf{W} \mathbf{G}^{-\top} : \dot{\mathbf{G}} + (\partial W / \partial \mathbf{A}) : \dot{\mathbf{A}} + (\partial W / \partial p) \dot{p}$  and substituting into (29) using (27, 28) provides

$$0 \leq \left( \mathbf{P} \mathbf{G}^\top - J_G \frac{\partial W}{\partial \mathbf{A}} \right) : \dot{\mathbf{A}} + \left( \mathbf{A}^\top \mathbf{P} + (g_s \Phi_s^0 - J_G W) \mathbf{G}^{-\top} \right) : \dot{\mathbf{G}} + \bar{G}_o^0 - \mathbf{J}_f^0 \cdot \text{Grad} g_f - \mathbf{J}_o^0 \cdot \text{Grad} g_o. \quad (30)$$



By the argument of [Coleman and Noll \(1963\)](#), the inequality (30) must hold for any admissible process. In particular, since  $\dot{\mathbf{A}}$  is arbitrarily prescribed, the following standard equalities must hold universally

$$\mathbf{P} = \frac{\partial W^0}{\partial \mathbf{A}} \mathbf{G}^{-\top} \quad \Leftrightarrow \quad \mathbf{T} = J_A^{-1} \mathbf{A} \frac{\partial W}{\partial \mathbf{A}} \quad (31)$$

which provides the standard stress-strain relation for a hyperelastic material. The resulting dissipation inequality,

$$0 \leq \left( \mathbf{A}^\top \mathbf{P} + (g_s \Phi_s^0 - J_G W) \mathbf{G}^{-\top} \right) : \dot{\mathbf{G}} + \bar{G}_o^0 - \mathbf{J}_f^0 \cdot \text{Grad } g_f - \mathbf{J}_o^0 \cdot \text{Grad } g_o, \quad (32)$$

highlights the different modes of dissipation in the system, coming from distinct biophysical processes, specifically growth and transport. Thus, these contributions must satisfy (32) individually, hence

$$(g_s \Phi_s \mathbf{1} - \mathbf{B}) : \mathbf{L}_G \geq 0, \quad (33a)$$

$$\bar{G}_o^0 - \mathbf{J}_f^0 \cdot \text{Grad } g_f - \mathbf{J}_o^0 \cdot \text{Grad } g_o \geq 0. \quad (33b)$$

Here,  $\mathbf{B} := W \mathbf{1} - J_A \mathbf{A}^\top \mathbf{T} \mathbf{A}^{-\top}$  denotes the Eshelby stress tensor, which appears as an important quantity for growth ([Epstein and Maugin, 2000](#); [Vandiver and Goriely, 2009](#)).

### 2.3.2. Growth law

We discuss the constitutive law for the growth of the cell matrix. Focusing on the solid component, we first decompose the stress additively into a solid and fluid part as  $\mathbf{T} = \mathbf{T}_s - \phi p \mathbf{1}$  where  $\mathbf{T}_s$  is the partial stress due to the solid component ([Coussy, 2003](#); [Preziosi and Farina, 2002](#)):

$$\mathbf{T}_s = J_A^{-1} \mathbf{A} \frac{\partial \Psi_s}{\partial \mathbf{A}} - \phi_s p \mathbf{1}. \quad (34)$$

We can rewrite (35) in terms of the partial Eshelby stress  $\mathbf{B}_s := \Psi_s \mathbf{1} - \phi_s J_A \mathbf{A}^\top \mathbf{T}_s \mathbf{A}^{-\top}$  ( $= \mathbf{B}$ ) as

$$(g_s \Phi_s \mathbf{1} - \mathbf{B}_s) : \mathbf{L}_G \geq 0. \quad (35)$$

This dissipation inequality expresses a thermodynamic constraint on the growth law. In particular, the case  $g_s = 0$ , where the solid is added with no energy to the matrix, defines a *passive* growth process ([Goriely, 2017](#)). Generally, from (35), a natural path is then to adopt the Eshelby stress  $\mathbf{B}_s$  as a driving force for growth. A common approach then is to postulate the existence of a homeostatic stress  $\mathbf{B}^*$  such that  $\mathbf{B}^* : \mathbf{L}_G = \Phi_s g_s \Gamma$ , so a natural growth law can be chosen of the general form  $\mathbf{L}_G = \mathcal{H} : (\mathbf{B}^* - \mathbf{B}_s)$  with  $\mathcal{H}$  a fourth-order extensibility tensor such that the inequality holds for any  $\mathbf{B}_s$  ([Ambrosi and Guana, 2007](#); [Ambrosi et al., 2012](#); [DiCarlo and Quiligotti, 2002](#); [Dunlop et al., 2010](#); [Tiero and Tomassetti, 2016](#); [Xue et al., 2016](#)). In plants however, it is unlikely that such homeostatic stress is actively maintained. Instead, the growth of plant cell walls is generally seen as a passive, plastic-like process ([Ali and Traas, 2016](#); [Barbacci et al., 2013](#); [Dyson et al., 2012](#)) which involves complex anisotropies and nonlinear threshold effects ([Boudon et al., 2015](#); [Oliveri et al., 2018](#)). Whether simple growth laws based on the Eshelby stress can reproduce basic properties of plant matter remains unclear to us. Thus, we reserve this problem for another occasion and instead adopt a simpler, phenomenological approach. Indeed, *strain*-based growth laws

of the form  $\mathbf{L}_G = \mathcal{G}(\mathbf{A})$  have been adopted (Boudon et al., 2015; Bozorg et al., 2016; Kelly-Bellow et al., 2023; Laplaud et al., 2024; Mosca et al., 2024; Rojas et al., 2011; Zhao et al., 2020), where typically, the cell walls expand once they surpass a certain strain threshold. These growth laws are relatively simple to parameterise and capture elegantly some observed phenomenological properties of plant matter, for example the commonly-accepted fact that growth is slower in rigid tissues or along the direction of load-bearing cellulose microfibrils (all other things being equal).

Following previous strain-based models we postulate a strain-based growth law where we assume that during growth, the strain is maintained close to a strain threshold  $\mathbf{E}^*$ . Therefore, we posit a linear growth law of the form

$$\mathcal{G}(\mathbf{A}) = \mathcal{K} : (\mathbf{E} - \mathbf{E}^*)_+, \quad (36)$$

with  $\mathcal{K}$  a fourth-order tensor controlling the rate and anisotropy of the growth (with unit inverse time);  $\mathbf{E} := (\mathbf{A}^\top \mathbf{A} - \mathbf{1})/2$  the symmetric Lagrangian elastic tensor;  $\mathbf{E}^*$  is a threshold strain tensor; and  $(\cdot)_+$  is an invariant extension of the ramp function to symmetric tensors, that is, for any symmetric tensor  $\mathbf{S}$  with eigenvalues  $S_i$  and corresponding normalised eigenvectors  $\mathbf{s}_i$ , we define  $(\mathbf{S})_+ := \max(0, S_i) \mathbf{s}_i \otimes \mathbf{s}_i$ . For comparison, (36) is a generalisation of the growth law introduced by Boudon et al. (2015).

Note that there is no guarantee anymore that the dissipation inequality (35),

$$g_s \Phi_s \geq \frac{\mathbf{B}_s : \mathcal{G}(\mathbf{A})}{\text{tr}(\mathcal{G}(\mathbf{A}))}, \quad (37)$$

will be always satisfied with  $g_s = 0$ . (However, in practice, the r.h.s. appears to be indeed negative in many cases studied here.) We conclude that strain-based growth processes may not be universally passive. We note that, recently, some authors have proposed that material insertion and pectin expansion may also drive growth, independently of turgor (Haas et al., 2020, 2021). This hypothesis, albeit contentious (Cosgrove and Anderson, 2020), implies that growth in plant cell walls may be—at least partly—an active process.

### 2.3.3. Transport

Next, we discuss the second inequality (33b) for the material fluxes. Using  $\mathbf{J}_o^0 = J\phi_o \mathbf{F}^{-1} \mathbf{w}_o$  and  $\mathbf{J}_f^0 = J\phi_f \mathbf{F}^{-1} \mathbf{w}_f$  and postulating an active transport contribution of the form  $\bar{\mathbf{g}}_o = \phi_o \bar{\mathbf{f}}_o \cdot \mathbf{w}_o$  with  $\bar{\mathbf{f}}_o$  an effective force sustaining active transport, (33b) becomes

$$-\phi_f \mathbf{w}_f \cdot \text{grad } g_f + \phi_f \mathbf{w}_o \cdot (\bar{\mathbf{f}}_o - \text{grad } g_o) \geq 0. \quad (38)$$

To make progress, we introduce Onsager's reciprocal relations (Martyushev and Seleznev, 2006; Onsager, 1931; Xue et al., 2016)

$$-\phi_f \text{grad } g_f = L_{fo}(\mathbf{v}_f - \mathbf{v}_o) + \mathbf{L}_{fs}(\mathbf{v}_f - \mathbf{v}) = -L_{fo} \mathbf{w}_o + (\mathbf{L}_{fs} + L_{fo} \mathbf{1}) \mathbf{w}_f, \quad (39a)$$

$$\phi_o \bar{\mathbf{f}}_o - \phi_o \text{grad } g_o = L_{of}(\mathbf{v}_o - \mathbf{v}_f) + \mathbf{L}_{os}(\mathbf{v}_o - \mathbf{v}) = -L_{of} \mathbf{w}_f + (\mathbf{L}_{os} + L_{of} \mathbf{1}) \mathbf{w}_o, \quad (39b)$$

where  $L_{of} = L_{fo}$  is a fluid-osmolyte drag coefficient; and  $\mathbf{L}_{os}$  and  $\mathbf{L}_{fs}$  are positive-definite symmetric second-order tensors that characterise the anisotropic osmolyte-solid and fluid-solid drags, respectively, to reflect the anisotropic structure of the solid matrix. Indeed, substituting (39) into

(38) gives  $\mathbf{w}_f \cdot (\mathbf{L}_{fs} \mathbf{w}_f) + \mathbf{w}_o \cdot (\mathbf{L}_{os} \mathbf{w}_o) + L_{fo}(\mathbf{w}_f - \mathbf{w}_o)^2 \geq 0$ , which is always satisfied. These relations may be viewed as a generalisation of Fick's law to several transported species. Inverting (39) and using the Gibbs-Duhem equality  $\phi \text{grad } p = \phi_f \text{grad } g_f + \phi_o \text{grad } \phi_o$  we obtain the relative velocities

$$\mathbf{w}_f = \left[ \mathbf{L}_{os} \mathbf{L}_{fs} + L_{of}(\mathbf{L}_{os} + \mathbf{L}_{fs}) \right]^{-1} \left[ \phi_o (L_{fo} \bar{\mathbf{f}}_o + \mathbf{L}_{os} \text{grad } \phi_o) - \phi (\mathbf{L}_{os} + L_{of} \mathbf{1}) \text{grad } p \right], \quad (40a)$$

$$\mathbf{w}_o = (\mathbf{L}_{os} + L_{of} \mathbf{1})^{-1} (\phi_o \bar{\mathbf{f}}_o - \phi_o \text{grad } g_o + L_{fo} \mathbf{w}_f). \quad (40b)$$

In particular, in the limit of high osmolyte-solid drag  $\mathbf{L}_{os} \gg \mathbf{L}_{fs}, L_{of}$ , we derive

$$\mathbf{w}_f \approx (\mathbf{L}_{fs} + L_{of} \mathbf{1})^{-1} (\phi_o \text{grad } \phi_o - \phi \text{grad } p), \quad \mathbf{w}_o \approx \phi_o \mathbf{L}_{os}^{-1} (\bar{\mathbf{f}}_o - \text{grad } g_o). \quad (41)$$

Biologically, this assumption expresses the idea that in the absence of active transport, the osmolytes remain mostly confined within the cells (with some slow diffusive leakage) and are not convected by the fluid. Following Xue et al. (2016), the drag coefficients are given as  $\mathbf{L}_{fs} = \phi \mathbf{K}^{-1}$  and  $L_{of} = R_g \theta c_o / D_o$ , with  $\mathbf{K}$  the second-order symmetric *permeability tensor* that characterises the permeability of the mixture to the fluid (expressed in unit area per pressure per time);  $c_o$  is the molar concentration of osmolytes;  $D_o$  is the diffusivity of the osmolytes in the fluid; and  $R_g$  the universal gas constant. The chemical potential  $g_o$  of the solutes can be related to their molar concentration  $c_o$  in the fluid through

$$g_o = g_o^0 + \frac{R_g \theta}{v_o} \ln (c_o / c_o^0), \quad (42)$$

with  $v_o$  the molar volume of the osmolytes; and  $g_o^0$  and  $c_o^0$  are reference values, taken to be constant. Using the formulae  $\mathbf{j}_f = \phi_f \mathbf{w}_f$  and  $c_o = \phi_o / v_o \phi$  with (41, 42), we obtain finally

$$\mathbf{j}_f \approx \phi_f \left( \mathbf{K}^{-1} + \frac{R_g \theta c_o}{D_o \phi} \mathbf{1} \right)^{-1} \text{grad} (R_g \theta c_o - p). \quad (43)$$

For small concentration, more specifically for  $R_g \theta c_o \ll D_o \phi \mathbf{K}^{-1}$ , we recover a Darcy-type law

$$\mathbf{j}_f \approx -\phi_f \mathbf{K} \text{grad } \psi, \quad (44)$$

where  $\psi = p - \pi$  as in (1); with the osmotic pressure  $\pi$  given by the van 't Hoff relation  $\pi := R_g \theta c_o$ . Combining (10, 11, 16, 44) we can finally derive

$$\text{div} [\mathbf{v} + \mathbf{j}_o - (1 - \phi_o - \Phi_s / J_A) \mathbf{K} \text{grad } \psi] = \xi_s + \xi_o + \xi_f. \quad (45)$$

In our context, a useful simplification comes from the fact that, in plants, the fluid content actually accounts for most of the volume of the mixture, thus, water mass balance is barely affected by the small volume of the osmolyte and the cell walls. Therefore, we next take  $\xi_s \ll \xi_f$ ,  $\mathbf{j}_o \ll \mathbf{j}_f$ ,  $\phi_o, \phi_s \ll \phi$  and  $\mathbf{T}_s \approx \mathbf{T} + p \mathbf{1}$ .

#### 2.4. A closed system of equations

Combining (6, 15, 17, 36, 45), we obtain the following system of equations:

$$\operatorname{div}(\mathbf{v} - \mathbf{K} \operatorname{grad} \psi) = \xi_f, \quad (46a)$$

$$\frac{\partial \phi_o}{\partial t} + \operatorname{div}(\phi_o \mathbf{v} + \mathbf{j}_o) = \xi_o, \quad (46b)$$

$$\operatorname{div} \mathbf{T}_s + \mathbf{b} = \operatorname{grad} p, \quad (46c)$$

$$\mathbf{T}_s = \mathbf{T}_s^\top, \quad (46d)$$

$$\mathbf{F} = \mathbf{A} \mathbf{G}, \quad (46e)$$

$$\mathbf{L}_G = \mathcal{K} : (\mathbf{E} - \mathbf{E}^*)_+, \quad (46f)$$

$$\mathbf{T}_s = J_A^{-1} \mathbf{A} \frac{\partial \Psi_s}{\partial \mathbf{A}}, \quad (46g)$$

$$\psi = p - R_g \theta \phi_o / v_o. \quad (46h)$$

In total, we have a closed system of thirty-three partial-differential equations for thirty-three variables: the nine components of  $\mathbf{A}$ , the nine components of  $\mathbf{G}$ , the three components of  $\chi$ , the nine components of  $\mathbf{T}_s$ , and the three scalar variables  $p$ ,  $\psi$  and  $\phi_o$ .

#### 2.5. Boundary conditions

This system must be equipped with appropriate boundary conditions. Defining the outer normal  $\mathbf{n}$  to the boundary  $\partial \mathcal{B}$ , typical boundary conditions encountered in our context describing the flux of water through the boundary are Robin boundary conditions of the form

$$\mathbf{j}_f \cdot \mathbf{n} = -(\mathbf{K} \operatorname{grad} \psi) \cdot \mathbf{n} = k(\psi^* - \psi) \quad \text{on } \partial \mathcal{B}, \quad (47)$$

expressing a flux across the boundary due to a difference of water potential with the outside  $\psi^*$ , where  $k$  is the interfacial hydraulic conductivity. No-flux boundary conditions  $(\mathbf{K} \operatorname{grad} \psi) \cdot \mathbf{n} = 0$  are a particular case of (47). Note that when  $k \rightarrow \infty$ , the condition (47) simplifies to a Dirichlet constraint

$$\psi = \psi^* \quad \text{on } \partial \mathcal{B}. \quad (48)$$

Similarly, the mass balance equation for the osmolytes may be equipped with Dirichlet (fixing  $c_o$  at the boundary) or flux boundary condition. The usual boundary condition for the stress (46c) is

$$\mathbf{T} \mathbf{n} = \mathbf{t}_0 \quad \text{on } \partial \mathcal{B}, \quad (49)$$

with  $\mathbf{t}_0$  the applied traction density.

## 2.6. Apparent elasticity of a growing tissue

Given a solution to the system, an adscitious problem is to characterise the effective elasticity of the turgid tissue subject to residual stresses. Indeed, at timescales shorter than that of growth and water transport, water is effectively trapped in the tissue and the mixture can then be seen as a macroscopically *incompressible* hyperelastic material. Given a field of elastic pre-deformation  $\mathbf{A}$  and pressure  $p$ , the effective strain energy function of the mixture with respect to an incremental, superimposed deformation  $\hat{\mathbf{A}}$  is

$$\hat{W}(\hat{\mathbf{A}}, \hat{p}) = J_A^{-1} W(\hat{\mathbf{A}}\mathbf{A}, p) - \hat{p}(\det \hat{\mathbf{A}} - 1), \quad (50)$$

where  $\hat{p}$  is an undetermined Lagrange multiplier that accounts for the incompressibility constraint  $\det \hat{\mathbf{A}} = 1$ . The associated Cauchy stress is then

$$\hat{\mathbf{T}} = \hat{\mathbf{A}} \frac{\partial \hat{W}}{\partial \hat{\mathbf{A}}} = \mathbf{T}(\hat{\mathbf{A}}\mathbf{A}, p) - \hat{p}\mathbf{1}. \quad (51)$$

This expression is useful to describe the overall elastic response of the system to external forces, e.g. in the context of compression experiments performed on entire tissues (Hamant et al., 2008; Pieczywek and Zdunek, 2017; Robinson and Kuhlemeier, 2018; Zhu and Melrose, 2003), or to explore mechanical stability under growth-induced differential stresses or external loads (Ben Amar and Goriely, 2005; Vandiver and Goriely, 2008).

## 3. Longitudinal growth: hydraulic competition and growth-induced water gradients

### 3.1. General problem

To illustrate the behaviour of the system, we first examine the simple scenario of a growing, straight cylindrical rod so we reduce the system (46) to one dimension. We define  $s$ ,  $S$  and  $S_0$ , the arc lengths in the current, intermediate and initial configurations respectively. The associated total, growth and elastic stretches are  $\lambda := \partial s / \partial S_0$ ,  $\gamma := \partial S / \partial S_0$  and  $\alpha := \partial s / \partial S$ , with  $\lambda = \alpha\gamma$  (6). From (4, 8), we derive

$$\frac{\partial v}{\partial s} = \frac{\dot{\alpha}}{\alpha} + \frac{\dot{\gamma}}{\gamma}, \quad (52)$$

with  $v$  the longitudinal Eulerian velocity (positive towards increasing  $s$ ). Assuming that the rod is unloaded, the balance of linear momentum (46c) for the axial partial stress  $t_s$  yields  $t_s = p$ . System (46) then reduces to

$$\frac{\partial}{\partial s} \left( v - K \frac{\partial \psi}{\partial s} \right) = \xi_f, \quad (53a)$$

$$\frac{\partial \phi_o}{\partial t} + \frac{\partial}{\partial s} (\phi_o v + j_o) = \xi_o, \quad (53b)$$

$$\frac{\partial v}{\partial s} = \frac{1}{2\tau} (\alpha^2 - \alpha^{*2})_+ + \frac{\partial \alpha}{\partial t} + \frac{v}{\alpha} \frac{\partial \alpha}{\partial s}, \quad (53c)$$

$$p = \frac{\partial \Psi_s}{\partial \alpha}, \quad (53d)$$

$$\psi = p - R_g \theta \phi_o / v_o, \quad (53e)$$

where  $\tau$  is the characteristic time of wall synthesis during growth (i.e.  $\mathcal{K} = 1/\tau$ );  $\mathbf{K} = K$  is the permeability coefficient; and  $\mathbf{j}_0 = j_0$  is the osmolyte flux.

For simplicity, we focus in this section on infinitesimal elastic deformations and define  $\epsilon = \alpha - 1$  the *infinitesimal strain*, with  $\epsilon \ll 1$ , and the strain threshold  $\epsilon^* = \alpha^* - 1 \geq 0$ . Thus, Hooke's law provides

$$p = E\epsilon, \quad (54)$$

with  $E$  the effective Young's modulus of the solid. Here we assume that the osmotic pressure  $\pi$  is maintained constant w.r.t  $s$  and  $t$ , so we elide (53b, 53e) and substitute  $\partial\psi/\partial s = \partial p/\partial s$  into (53a). Similarly, we take  $K$ ,  $\epsilon^*$ , and  $\tau$  constant and homogeneous. Indeed, the focus here is on the role of a spatially heterogeneous stiffness, which has been linked experimentally (Kierzkowski et al., 2012) and theoretically (Alonso-Serra et al., 2024; Boudon et al., 2015; Cheddadi et al., 2019) to organ patterning in development. Therefore, we allow the rigidity to vary spatially as  $E(s, t) = E_0 f(s)$  with  $f$  a dimensionless function of order unit, and  $E_0$  a characteristic Young's modulus of the rod. Finally, taking  $\tau$ ,  $E_0$  and  $\sqrt{KE_0\tau}$  as reference time, pressure and length, respectively, we can nondimensionalise the system through the substitutions

$$\tilde{v} = v \sqrt{\frac{\tau}{KE_0}}, \quad \tilde{s} = \frac{s}{\sqrt{KE_0\tau}}, \quad \tilde{t} = \frac{t}{\tau}, \quad \tilde{\xi}_f = \xi_f \tau, \quad \tilde{p} = \frac{p}{E_0}. \quad (55)$$

In particular, the length  $\mathcal{L}_h := \sqrt{KE_0\tau}$  defines the characteristic *hydromechanical length* of the system. Altogether, we obtain to  $O(\epsilon)$ :

$$\frac{\partial \tilde{v}}{\partial \tilde{s}} = \frac{\partial^2 \tilde{p}}{\partial \tilde{s}^2} + \tilde{\xi}_f, \quad (56a)$$

$$\frac{\partial \tilde{v}}{\partial \tilde{s}} = (\epsilon - \epsilon^*)_+ + \frac{\partial \epsilon}{\partial \tilde{t}} + \tilde{v} \frac{\partial \epsilon}{\partial \tilde{s}}, \quad (56b)$$

with  $\tilde{p} = f\epsilon$ . To simplify notations, we drop the tildes and use nondimensionalised variables. For comparison, this system resembles the static model of Plant (1982), and extends the Lockhart-Cosgrove-Ortega model (1, 2) to a one-dimensional continuum. Note also that the r.h.s of (37) is always negative or zero here, thus, by the argument of Section 2.3.2, our strain-based growth law is compatible with a passive growth process. In the next two sections, we study the effect of heterogeneous elastic moduli on the growth behaviour of the rod.

### 3.2. Material heterogeneity and hydraulic competition

Here we are interested in the boundary effects arising between two regions with different mechanical properties, specifically the effect of different stiffnesses. Therefore, we consider a rod with initial arclength  $S_0 \in [-L_0/2, L_0/2]$ , divided in the middle into two part of different rigidity, that is, we posit the rigidity field given by

$$f(s(S_0)) = 1 - \eta\theta(S_0), \quad (57)$$

where  $0 \leq \eta < 1$  denotes the stiffness step at the interface  $s = 0$ ; and with  $\theta$  the Heaviside step function (i.e.  $\theta(x) = 0$  if  $x < 0$  and  $\theta(x) = 1$  if  $x \geq 0$ ). The region  $S_0 > 0$  is softened, with stiffness  $1 - \eta$ , with respect to the base stiffness equal to unity. Assuming  $s(0) = v(0) = 0$ , without loss of generality (i.e. considering an observer located at the interface), we have  $f(s) = 1 - \eta\theta(s)$ . Here we assume no-flux boundary conditions at both ends of the domain, however we allow water entry through a bulk source  $\xi_f = k(p^* - p)$ , with  $k$  the effective permeability with the outside, and  $p^*$  a constant base effective pressure, encompassing the excess osmolarity relative to the outside, and the outer hydrostatic pressure.

To gain insight into the shape of the solutions, we focus on the steady regime, i.e. on self-similar stationary solutions on an infinite line. On setting  $\partial\epsilon/\partial t = 0$  in (56), the problem reduces to:

$$v' = p'' + k(p^* - p), \quad (58a)$$

$$v' = (\epsilon - \epsilon^*)_+ + v\epsilon', \quad (58b)$$

with the apostrophe denoting derivative with respect to  $s$ , and where  $p = f\epsilon$ . To make progress, we consider a small perturbative softening  $\eta \ll 1$ . Therefore we expand all variables as power series of  $\eta$ , i.e.  $p = p_0 + \eta p_1 + \dots$ ,  $\epsilon = \epsilon_0 + \eta \epsilon_1 + \dots$  and  $v = v_0 + \eta v_1 + \dots$ , and then treat each order in (58) separately. To ease calculations, it is also convenient here to ignore the threshold effect in (58b) and assume  $p^* \geq \epsilon \geq \epsilon^*$ . The base solution at  $O(1)$  has uniform pressure and velocity gradient and is given by

$$p_0 = \epsilon_0 = \frac{\epsilon^* + kp^*}{1 + k}, \quad (59a)$$

$$v_0 = as, \quad \text{with} \quad a = \frac{p^* - \epsilon^*}{1 + k^{-1}}. \quad (59b)$$

Unsurprisingly,  $p_0$  can be identified to the Lockhart pressure (3). At  $O(\eta)$ , we have

$$v'_1 = p'_1 - kp_1, \quad v'_1 = \epsilon_1 + v_0\epsilon'_1. \quad (60)$$

Eliminating  $v'_1$  and using  $p_1 = \epsilon_1 - \epsilon_0\theta(s)$  and  $p_0 = \epsilon_0$ , we obtain a single equation for  $p_1$ ,

$$p'_1 - asp'_1 - (1 + k)p_1 = p_0\theta(s), \quad (61)$$

defined on both regions  $s < 0$  and  $s > 0$ . A general solution to this equation can be expressed in terms of the Kummer confluent hypergeometric function  ${}_1F_1$ , the gamma function  $\Gamma$  and the Hermite polynomials (of the first kind)  $H_\lambda$ . By imposing the condition that pressure must be bounded and continuously differentiable at  $s = 0$ , we can determine the four integration constants and obtain the compound asymptotic solution

$$p(s) = p_0 + \frac{\eta p_0}{k + 1} \left[ \frac{\pi \csc(\pi c)}{\Gamma(c/2)\Gamma(1-c)} H_{-c}(s\sqrt{a/2}) - \theta(s) - \theta(-s)h_{-c}(s\sqrt{a/2}) \right] + O(\eta^2), \quad (62)$$

with  $c := (k + 1)/a$ ; and  $h_\lambda = {}_1F_1(-\lambda/2; 1/2; x^2)$  the Hermite functions ( $\pi$  denotes here the ratio of a circle's circumference to its diameter). The expansion rate  $v'$  is obtained directly by substituting this expression into (58a).



Example solutions are shown in Fig. 2. As can be seen, the softening of the right-hand-side region results in a pressure drop in that region, reflecting the reduced mechanical resistance of the cell walls to water entry. As pressure decreases smoothly at the junction between the soft to the stiff region, the elongation rate  $v'$  jumps discontinuously, reaching a global minimum at  $s = 0^-$  and a maximum at  $s = 0^+$ . This jump directly results from the strain-based growth law, and the strain discontinuity at  $s = 0$ . Due to the pressure gradient, water seeps towards increasing  $s$ , i.e. from the stiff region to the soft region. The characteristic length of this seepage,  $L_c := -p'(0)/2\Delta p \leq 1$ , increases when external water supply  $k$  decreases, as illustrated by the inset in Fig. 2(a). This result shows the emergence of hydraulic competition between the two regions. This competition concerns a larger portion of the tissue when external water supply becomes small. The presence of an external source of water  $k$  also tends to reduce the difference in pressure between the two regions (thus the seepage), as can be seen from the pressure drop  $\Delta p = \eta p_0 / (1 + k)$  between the two asymptotes  $s = -\infty$  and  $s = +\infty$ . This gap is maximal when  $k \ll 1$ , where water becomes scarce, with

$$p(s) = \epsilon^* - \frac{\eta}{2} (\theta(-s)e^s + \theta(s)(2 - e^{-s})) + O(\eta^2). \quad (63)$$

In this limit example however, the volume of water in the rod is conserved, thus as the right-hand side region grows along a region of effective size unity, the other side, which is actually under the growth threshold, has to shrink (thus this limit is actually nonphysical). This issue is addressed later in Section 3.3. For comparison, Fig. 2 also shows the case where internal fluxes along the rod are suppressed ( $K = 0$ ), illustrated by the dashed lines. In this case, the pressure and the velocity gradient are piece-wise continuous, with

$$p(s) = p_0 - \frac{\eta p_0 \theta(s)}{k + 1} + O(\eta^2), \quad v'(s) = a + \frac{\eta p_0 \theta(s)}{1 + k^{-1}} + O(\eta^2), \quad (64)$$

corresponding to the asymptotes for the general case. In the general case where the two regions exchange water, this jump in expansion rate  $v'$  across the interface is amplified by a factor  $1 + k^{-1}$  with respect to the situation with zero flux. In particular, in situations where water supply is impeded (i.e.  $k \ll 1$ ) and the overall growth becomes slower, this amplification factor diverges as the effect of hydraulic competition becomes more visible. In other words, although one might initially expect that water movements along the rod would serve to smooth out heterogeneities, we show that, near the interface ( $|s| \lesssim L_c$ ), the combined effects of growth, hydraulics and mechanics actually accentuates the effect of heterogeneous mechanical properties on the growth dynamics. Interestingly, such effects have been proposed to play a role in the initiation of organs in the shoot apical meristem Alonso-Serra et al. (2024) (see Section 6).

### 3.3. Water gradient in apically growing organs

Plant shoots and roots grow typically along an elongating apical region (Erickson, 1976), while the rest of the tissue stiffens and stops growing. Kinematically, this type of growth is akin (but not physically equivalent) to tip growth. Here, we explore the existence of tip-like, self-similar solutions to our system. Therefore, we focus on the steady regime (58), and define  $s$ , the arclength

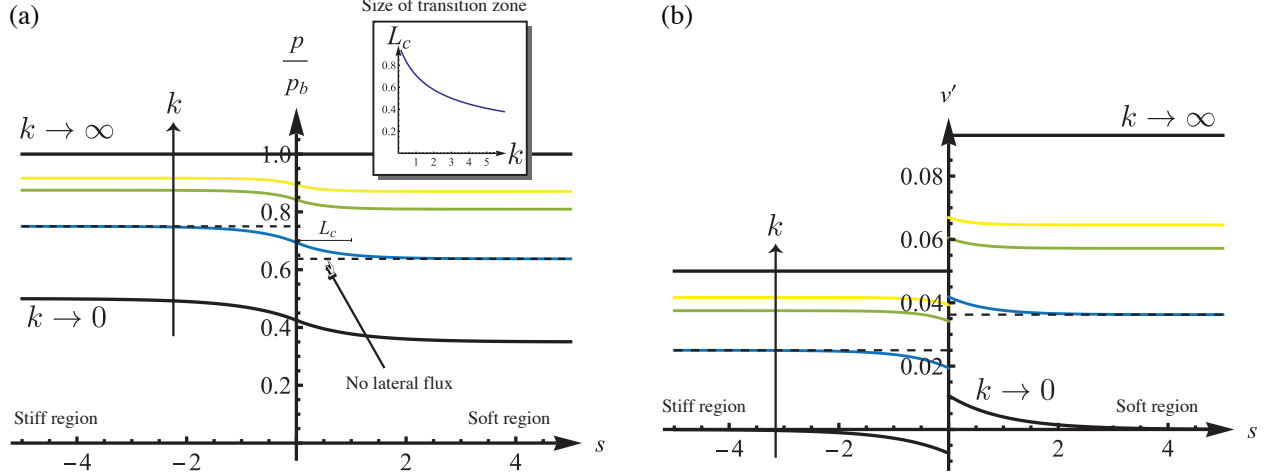


Figure 2: Asymptotic solution for small softening  $\eta \ll 1$ : (a) normalised pressure  $p(s)/p^*$  and (b) expansion rate  $v'(s)$ , shown for different values of the effective permeability with the outside  $k$ . Solid black lines show the limit cases  $k \rightarrow 0$  (closed system) and  $k \rightarrow \infty$ . Dashed lines show the case where flux is suppressed between the two regions. Inset shows the size of the transition zone  $L_c$  as a function of  $k$ . Parameters:  $\eta = 0.3$ ,  $p^* - \epsilon^* = 0.05$ ,  $k = 1, 3, 5$ .

measured from the apex of the plant towards the base. In this scenario,  $v$  is then the velocity of the domain measured in the co-moving frame attached to the apex.

To illustrate the role of chemical growth regulation in our framework, we here assume that growth is controlled by a growth hormone (e.g. auxin) with concentration  $\rho$ . We posit that the hormone is actively convected with velocity  $v_a$  from the apex ( $s = 0$ ) towards the base ( $s = \infty$ ), diffuses with diffusion coefficient  $D$  and is reabsorbed with rate constant  $\beta$ . In the steady regime, the concentration profile obeys

$$D\rho'' - (v + v_a)\rho' - (v' + \beta)\rho = 0. \quad (65)$$

In the convection-dominated regime  $D\rho', v\rho \ll v_a\rho$ , the hormone concentration is given by  $\rho(s) = \rho_0 e^{-s/\sigma}$ , where  $\rho_0 := \rho(0)$  is the concentration at the apex; and where  $\sigma := \beta/v_a$  sets the length scale for the hormonal regulation (Moulton et al., 2020). In plants, transported hormones such as auxin are involved in the control of cell wall elastic properties (Sassi et al., 2014). Therefore, we assume that the effect of the hormone is to reduce the elastic modulus of the tissue. Assuming a small, linear effect of the hormone on the elastic modulus, we write

$$f \approx 1 - \eta\rho/\rho_0, \quad (66)$$

with  $\eta \ll 1$ . Note that an alternative mechanism producing a gradient in rigidity could be a gradual stiffening of the tissue as the cells age and move away from the apex (Eggen et al., 2011).

Firstly, we assume that no growth occurs in the absence of apical softening (i.e. if  $\eta = 0$ ), thus we choose  $\epsilon^* \geq p^*$ . Indeed, in Section 3.2, the choice  $\epsilon^* < p^*$  resulted in exponential growth, precluding then the possibility of tip-like growth regimes. As previously, we solve (58) asymptotically to first order in  $\eta$ . The base solution is  $p_0 = \epsilon_0 = p^*$  and  $v_0 = 0$ . At  $O(\eta)$ , we have

$$p_1'' - (1 + k)p_1 = p_0 e^{-s/\sigma}. \quad (67)$$

Here  $k$  can be interpreted biologically as a rate constant characterising the effective permeability between the growing tissue and the organ's vascular bundle. Note that (67) is valid only as long as the strain is above the growth threshold, i.e.  $\epsilon > \epsilon^*$ . Away from the tip, under this growth threshold, the system is in the purely elastic regime and obeys

$$p_1'' - kp_1 = 0. \quad (68)$$

The general solutions for (67, 68) can be obtained easily. The difficulty is then to determine the unknown arclength  $\Sigma$  at which the threshold is attained. Enforcing the condition that pressure  $p$  is bounded and continuously differentiable, and using  $\epsilon(\Sigma^-) = \epsilon(\Sigma^+) = \epsilon^*$  along with the no-flux condition at the tip  $p'(0) = 0$ , we can express all the integration constants as functions of  $\Sigma$ . The latter is ultimately identified as the root of some (slightly uncomely) transcendental equation which can be solved numerically, given values of  $k, \eta, \sigma, \epsilon^*$ , and  $p^*$ .

Fig. 3 shows example solutions. As can be seen in Fig. 3(a), the softening of the distal region results in a drop in pressure there. In the non-growing region (i.e. beyond the intersection point between the solid line and the dashed line), the pressure converges to its base value  $p^*$  as  $e^{-s\sqrt{k}}$ , i.e., perhaps surprisingly, there exists a water potential gradient of lengthscale  $k^{-1/2}$  resulting from the softening of the shoot over a length  $\sigma$ .

We can compute the tip velocity with respect to the base as  $v_\infty = v(\Sigma)$ , which is, as expected, a growing function of  $k$ ; see the inset in Fig. 3(b). In the limit case  $k \gg 1$ , with  $p = p^*$ , the apex grows along a region of maximal size  $\Sigma = \sigma \log(\eta\epsilon^*/(\epsilon^* - p^*))$ . This length is positive only if  $\eta > 1 - p^*/\epsilon^*$ , i.e. when the equilibrium pressure  $p^*$  is not too far from the growth threshold  $\epsilon^*$ , given a certain level of softening  $\eta$ , otherwise the pressure is too low to produce any growth at all. The tip velocity is then maximal, given by

$$v_\infty \approx p^* \sigma (p^*/\epsilon^* - 1 + \eta) + \sigma (p^* - \epsilon^*) \log\left(\frac{\eta\epsilon^*}{\epsilon^* - p^*}\right). \quad (69)$$

Conversely, when  $k \rightarrow 0$ , the growth zone vanishes and  $v_\infty \rightarrow 0$ . In this case, the base of the plant located at  $s \rightarrow \infty$  is the only possible source of water but cannot sustain permanently the gradient in water potential necessary for growth. Both limit cases are plotted with solid black lines in Fig. 3.

### 3.4. Parameter estimates

The biological relevance of hydraulic gradients is predicated upon the ratio of hydromechanical length  $\mathcal{L}_h = \sqrt{KE\tau}$  to growth region size. To estimate this ratio, we consider a linear chain of identical Lockhart cells of average length  $\ell$  (maintained constant through cell-division), hydraulically-insulated from their environment, but exchanging water with their two adjacent neighbours with membrane conductivity  $\kappa$ . From dimensional considerations, we expect the bulk conductivity for this chain of cells to be  $K \sim \ell\kappa$ . We take  $\kappa = 10^{-8}$ – $10^{-7}$  m.s<sup>-1</sup>.MPa<sup>-1</sup> (Forterre, 2022; Laplaud et al., 2024). Taking the turgor pressure  $p$  to be of the order of 1 MPa (Long et al., 2020) and the strain  $\epsilon = 0.05$ , the bulk elastic modulus is  $E = p/\epsilon = 20$  MPa. Taking  $\ell = 10$   $\mu$ m and estimating  $\tau = 10^1$ – $10^3$  s, we obtain  $\mathcal{L}_h \approx 1$ – $10\ell$ ; namely, for this chain of cells, the length of interest for hydromechanical control is on the order of 1 to 10 cells. In practice, these values are very hard to measure with precision, and may vary a lot between different scenarios.

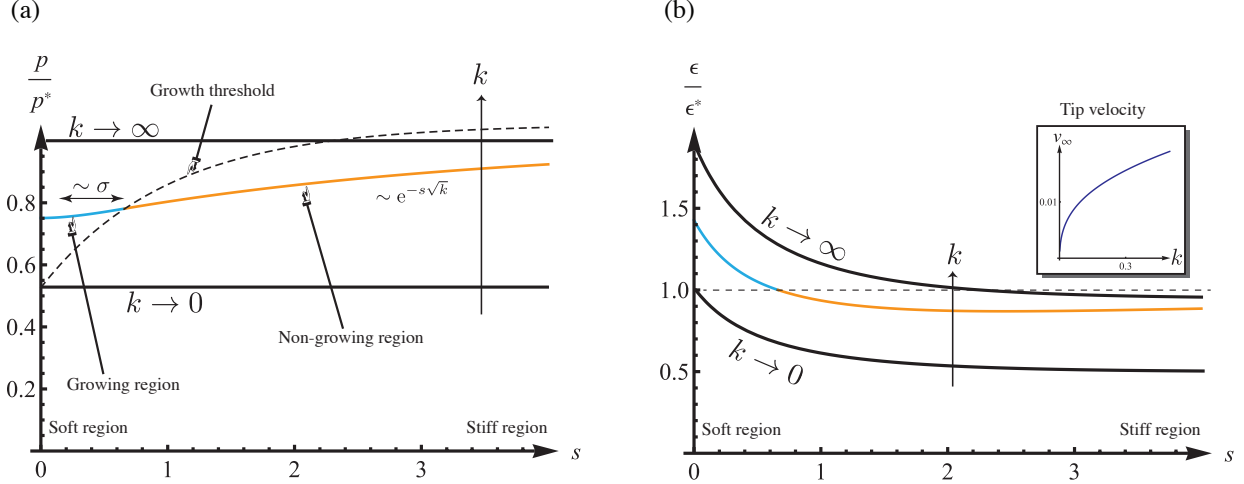


Figure 3: Asymptotic tip-like growth regimes for  $\eta \ll 1$ : (a) normalised pressure  $p(s)/p^*$  and (b) normalised strain  $\epsilon(s)/\epsilon^*$ , shown for different values of  $b$ . The parts of the curves plotted in blue are above the growth threshold and correspond to growing regions; those in orange are under the threshold and correspond to a purely elastic regime. Solid black lines show the limit cases  $k \rightarrow 0$  and  $k \rightarrow \infty$ . Dashed lines show the position of the growth threshold in pressure and strain space. Inset shows the tip velocity  $v_\infty$  as a function of  $k$ . Parameters:  $k = 0.1$ ;  $\epsilon^* = 0.1$ ;  $p^* = 0.095$ ;  $\sigma = 1$ ; and  $\eta = 0.5$ .

## 4. Growth of a cylinder: hydraulics and residual stress in stem development

### 4.1. Overview

We now move on to a fully three-dimensional, nonlinearly elastic scenario to study the growth of a cylindrical stem. Here, the focus is on the interplay between heterogeneous material properties, water fluxes, and growth in multiple dimensions, illustrating how hydraulic effects and differential material properties can constrain the growth and internal stresses within a simple three-dimensional structure.

### 4.2. Governing equations

We consider the growth of a cylinder of initial radius  $A$  and length  $L$ , and current radius  $a$  and length  $\ell$ . The initial domain is parameterised by the system of cylindrical coordinates  $(R, \Theta, Z)$ , with  $R$  the radial coordinate,  $\Theta$  the azimuthal angle, and  $Z$  the axial coordinate (Fig. 4). In an axisymmetric deformation, a point  $(R, \Theta, Z)$  in the reference configuration is moved to the location  $(r, \theta, z)$  in the current configuration. Thus, the deformation  $\chi$  is given explicitly by  $r = r(R, t)$ ,  $\theta = \Theta$ , and  $z = z(Z, t)$ , with

$$r(0, t) = 0, \quad z(0, t) = 0 \quad (70)$$

at  $R = 0$ . In virtue of the symmetry, we can identify the two orthonormal bases associated with both systems of cylindrical coordinates:  $\mathbf{E}_R = \mathbf{e}_r$ ,  $\mathbf{E}_\Theta = \mathbf{e}_\theta$  and  $\mathbf{E}_Z = \mathbf{e}_z$ . Further assuming that the gradient of deformation is invariant by  $Z$ , the problem is effectively one-dimensional and depends only on  $r$  and  $t$ . The deformation gradient is given by

$$\mathbf{F} = r' \mathbf{e}_r \otimes \mathbf{E}_R + \frac{r}{R} \mathbf{e}_\theta \otimes \mathbf{E}_\Theta + \frac{\ell}{L} \mathbf{e}_z \otimes \mathbf{E}_Z, \quad (71)$$

where the apostrophe denotes differentiation w.r.t.  $R$ ; and  $\otimes$  is the tensor product. The Eulerian and Lagrangian velocities are given respectively by  $\mathbf{v} = v \mathbf{e}_r + z \dot{\zeta} \mathbf{e}_z$  and  $\mathbf{V} = V \mathbf{e}_r + (Z \dot{\zeta} \ell / L) \mathbf{e}_z$ , with  $\dot{\zeta} := \dot{\ell} / \ell$  the relative rate of elongation. The growth and elastic tensors can be written in the cylindrical basis as  $\mathbf{G} = \text{diag}(\gamma_r, \gamma_\theta, \gamma_z)$  and  $\mathbf{A} = \text{diag}(\alpha_r, \alpha_\theta, \alpha_z)$ . By (6, 71), we have  $r' = \alpha_r \gamma_r$ ,  $r/R = \alpha_\theta \gamma_\theta$  and  $\ell/L = \alpha_z \gamma_z$ . The gradient of velocity can be related to the growth and elastic stretch rates through (4, 8)

$$\frac{\partial v}{\partial r} = \frac{\dot{\gamma}_r}{\gamma_r} + \frac{\dot{\alpha}_r}{\alpha_r}, \quad \frac{v}{r} = \frac{\dot{\gamma}_\theta}{\gamma_\theta} + \frac{\dot{\alpha}_\theta}{\alpha_\theta}, \quad \dot{\zeta} = \frac{\dot{\gamma}_z}{\gamma_z} + \frac{\dot{\alpha}_z}{\alpha_z}. \quad (72a)$$

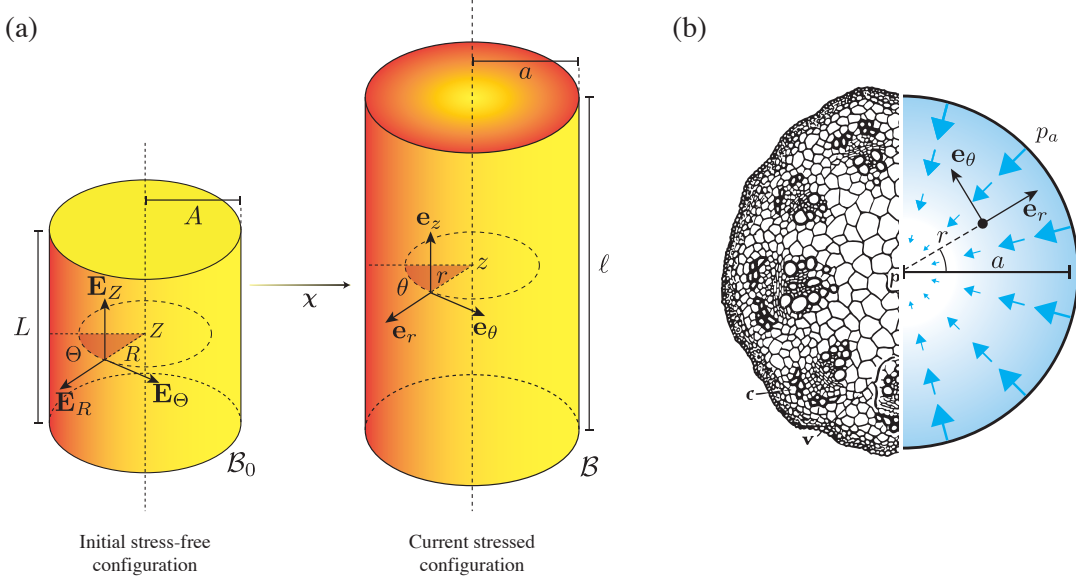


Figure 4: (a) Growth of a cylinder: initial and current configuration. (b) Hydraulic model for stem growth. Left: Cross-section of young stem of castor bean (*Ricinus communis*):  $e$  – epidermis;  $c$  – cortex;  $p$  – pith;  $v$  – vascular bundle (drawing reproduced from Curtis, 1914). Right: Schematic of the water fluxes in the cross-section. Water is supplied at the outer boundary, mimicking a vascular bundle located close to the epidermis.

By symmetry, the stress is also diagonal in the basis  $\{\mathbf{e}_r, \mathbf{e}_\theta, \mathbf{e}_z\}$ , with the total and partial Cauchy stresses given by  $\mathbf{T} = \text{diag}(T_r, T_\theta, T_z)$  and  $\mathbf{T}_s = \text{diag}(t_r, t_\theta, t_z)$ , respectively. The only non-vanishing component in the balance of momentum (46c) is then

$$\frac{\partial t_r}{\partial r} + \frac{t_r - t_\theta}{r} = \frac{\partial p}{\partial r}. \quad (73)$$

Assuming that the end caps are free and not subject to any load, we obtain the boundary condition for the stresses at the end caps (cf. Goriely, 2017, §11.8.3),

$$\int_0^a (t_z - p)r \, dr = 0. \quad (74)$$

Further, we assume that the outer pressure at  $r = a$  is zero, so (49) yields the condition

$$p(a) = t_r(a). \quad (75)$$

The balance of mass (46a) reads

$$\frac{1}{r} \frac{\partial}{\partial r} \left( rv - Kr \frac{\partial \psi}{\partial r} \right) + \dot{\zeta} = \xi_f, \quad (76)$$

where  $\mathbf{K} = K\mathbf{1}$ . The source  $\xi_f$  represents the water intake from a bulk vasculature modelled as a single reservoir with water potential  $\psi^*$ , i.e.  $\xi_f = k(\psi^* - \psi)$ . Assuming that the system is far from hydraulic equilibrium, i.e.  $\psi^* \gg \psi$ , we have  $\xi_f \approx k\psi^*$ , which is taken to be a function of  $r$  only. Thus (76) can be integrated directly as

$$v - K \frac{\partial \psi}{\partial r} = X_f - \frac{\dot{\zeta} r}{2}, \quad \text{with} \quad X_f(r) := \frac{1}{r} \int_0^r \xi_f(r') r' dr', \quad (77)$$

where we have used the no-flux regularity condition  $\partial \psi / \partial r = 0$ , and the geometric conditions  $r = 0$  and  $v = 0$  at  $R = 0$ . For simplicity, here we take  $\xi_f$  constant so that  $X_f = \xi_f r / 2$ . Similarly the osmotic pressure  $\pi$  is here assumed to not vary across the domain, so we elide the balance of osmolyte mass equation (15) and we take simply  $\partial \psi / \partial r = \partial p / \partial r$ . The cylinder exchanges water through its boundary at  $R = A$ , so we use the boundary condition (48)

$$\psi(a) = \psi_a \quad \Leftrightarrow \quad p(a) = p_a, \quad (78)$$

with  $p_a := \pi(a) + \psi_a$ . In the example treated next, we assume  $\xi_f = 0$  so that water enters the domain only through the boundary (however, for the sake of generality, we keep  $\xi_f$  in the following derivations). In plants, the organisation of the vascular bundle may vary considerably between species. The situation presented here mimics a type of architecture where the vascular bundle—xylem and phloem—is located near the epidermis, as illustrated in Fig. 4(b). For more complex vascular systems, we may assume a non-zero source  $\xi_f$ , or an additional water exchange point at  $R = 0$  (as in roots, where the vascular bundle is located generally near the centre). More in general, it is easy to extend the problem to the case of a vascular bundle placed at an arbitrary position  $r_v \in (0, a)$  by treating the two problems  $r < r_v$  and  $r > r_v$  separately (Passioura and Boyer, 2003).

The growth law (36) corresponds to

$$\frac{\dot{\gamma}_i}{\gamma_i} = \frac{1}{2\tau_i(R)} \left( \alpha_i^2 - \alpha^{*2} \right)_+, \quad (79)$$

with  $i \in \{r, \theta, z\}$ ; and  $\tau_r, \tau_\theta$  and  $\tau_z$  denote the characteristic times of material synthesis in the three separate directions of the cylinder. In growing stems, it is well known that heterogeneous material properties result in mechanical tension within the epidermis, a phenomenon called *tissue tension*, manifesting the existence of residual stresses. These stresses emerge from differential growth of the tissue, where the core grows relatively faster than the epidermis (Goriely et al., 2010; Holland et al., 2013; Kelly-Bellow et al., 2023; Peters and Tomos, 1996; Vandiver and Goriely, 2008). A classic experiment consists in peeling a stalk of rhubarb, which results in the detached cortex bending outward and shortening, along with rapid elongation of the exposed core when incubated in water (Holland et al., 2013; Kutschera, 1989; Kutschera et al., 1987; Kutschera and Niklas, 2007;

Sachs, 1865; Vandiver and Goriely, 2008), revealing tension in the cortex and compression below. This difference in growth rate is likely to be due to higher growth extensibility of the cell walls of the inner tissues (as exposed in Kutschera, 1989, and references therein). Therefore, we assume that the characteristic time  $\tau_z$  is larger near the epidermis than at the origin, so that, for equal strain levels, the epidermis undergoes slower growth. We posit  $\tau_z(R) = \tau_0 + \Delta\tau(R/A)^2$ , where  $\tau_0$  is the value at the origin, and  $\Delta\tau \geq 0$  defines the increment in  $\tau_z$  between the core and the epidermis.

Finally, the elastic constitutive equations read

$$t_i = \frac{\alpha_i}{J_A} \frac{\partial \Psi_s}{\partial \alpha_i}. \quad (80)$$

For simplicity, we here use an isotropic, compressible neo-Hookean strain energy function

$$\Psi_s(\alpha_r, \alpha_\theta, \alpha_z) = \frac{\mu}{2} (\alpha_r^2 + \alpha_\theta^2 + \alpha_z^2 - 3 - 2 \log(\alpha_r \alpha_\theta \alpha_z)) + \frac{\lambda}{2} (\alpha_\theta \alpha_r \alpha_z - 1)^2, \quad (81)$$

where the material coefficients  $\mu$  and  $\lambda$  identify to the Lamé coefficients in the linear regime. Note that in the limit of incompressibility ( $\lambda \gg 1$ ), no growth can occur since the solid cannot expand to absorb the fluid. Henceforth we set  $\lambda = \mu$  (corresponding to a Poisson ratio of 1/4 in the limit of linear elasticity). For simplicity, we assume that the elastic moduli are uniform (see Kutschera, 1989, and references therein). In fact, note that a heterogeneity in elastic rigidity would not be sufficient to capture differential growth on its own. Indeed, in a scenario where only  $\mu$  would be spatially heterogeneous, the axial stretch  $\alpha_z$  (thus the growth rate) would still be uniform in a cylindrical deformation.

As in Section 3, we can nondimensionalise the system using  $\sqrt{K\mu\tau_0}$ ,  $\tau_0$  and  $\mu$  as reference length, time and pressure, respectively. On eliminating  $\dot{\gamma}_\theta/\gamma_\theta$  and  $\dot{\gamma}_z/\gamma_z$  using (79), re-expressing the problem in the reference configuration, and rearranging the terms, we obtain a closed system of seven equations for the seven variables  $\gamma_r$ ,  $\alpha_r$ ,  $\alpha_\theta$ ,  $\alpha_z$ ,  $V$ ,  $r$ ,  $p$ , defined on the fixed domain  $\mathcal{B}_0$ :

$$r' = \alpha_r \gamma_r \quad (82a)$$

$$\frac{t'_r - p'}{r'} = \frac{t_\theta - t_r}{r}, \quad (82b)$$

$$\frac{p'}{r'} = \frac{1}{2} (\dot{\zeta} - \xi_f) r + V, \quad (82c)$$

$$\frac{\dot{\gamma}_r}{\gamma_r} = (\alpha_r^2 - \alpha^{*2})_+, \quad (82d)$$

$$\frac{\dot{\alpha}_r}{\alpha_r} + \frac{1}{2\tau_r} (\alpha_r^2 - \alpha^{*2})_+ = \frac{V'}{r'}, \quad (82e)$$

$$\frac{\dot{\alpha}_\theta}{\alpha_\theta} + \frac{1}{2\tau_\theta} (\alpha_\theta^2 - \alpha^{*2})_+ = \frac{V}{r}, \quad (82f)$$

$$\frac{\dot{\alpha}_z}{\alpha_z} + \frac{1}{2\tau_z} (\alpha_z^2 - \alpha^{*2})_+ = \dot{\zeta}, \quad (82g)$$



where  $t_r$  and  $t_\theta$  are given in terms of the elastic stretches via (80). This system is equipped with the boundary conditions (70, 75, 78) and the integral constraint (74) that is enforced via the undetermined parameter  $\dot{\zeta}$ . Note that (82b) has a geometric removable singularity at  $R = 0$  due to the boundary constraint  $r(0, t) = 0$ , which generates computational difficulties. This issue is easily alleviated by considering a perturbed boundary condition  $r(\epsilon, t) \approx \epsilon \alpha_r(\epsilon, t) \gamma_r(\epsilon, t)$  at  $R = \epsilon$ , where  $\epsilon \ll 1$ .

### 4.3. Analysis of the solutions

#### 4.3.1. Steady regime

Before solving the full dynamical problem, we first restrict our attention to steady growth regimes for which we enforce  $V = \dot{\alpha}_r = \dot{\alpha}_\theta = \dot{\alpha}_z = 0$  and  $\gamma_r = \gamma_\theta = 1$  (no radial growth). In this scenario, (82c) can be integrated directly, revealing that a permanent parabolic pressure profile is maintained across the elongating stem, as predicted by Passioura and Boyer (2003):

$$p - p_a = \frac{1}{4}(\dot{\zeta} - \xi_f)(r^2 - a^2). \quad (83)$$

In particular, this pressure is non-negative if

$$a^2 \leq \frac{4p_a}{\dot{\zeta} - \xi_f}; \quad (84)$$

otherwise, the radius is too large to allow for even distribution of water given the elongation rate  $\dot{\zeta}$ , and a zone of negative pressure forms at the centre of the stem. Eq. (84) may be viewed as a scaling constraint on growth, linking the kinematics ( $\dot{\zeta}$ ) and geometry ( $a$ ), for a given water supply ( $p_a, \xi_f$ ).

The rest of the system can be solved numerically (Appendix A). Fig. 5(a–c) illustrate the steady solution and its dependency on the (nondimensionalised) stem radius  $A$  and the parameter  $\Delta\tau$ . The density map in Fig. 5(a) shows the difference in axial stress  $T_z$  measured between the epidermis ( $R = A$ ) and the origin ( $R = 0$ ), with red indicating states of epidermal tension where  $T_z(A) > T_z(0)$ , and dashed line showing the level set  $T_z(A) = T_z(0)$ . We show three cross-sections of the stem showing the stress distribution  $T_z$  in three cases: 1–uniform  $\tau_z$ ; 2–heterogeneous  $\tau_z$  and thin stem; and 3–heterogeneous  $\tau_z$  and thicker stem. Fig. 5(b, c) show respectively the elongation rate  $\dot{\zeta}$  and mean pressure, in the  $A$ - $\Delta\tau$  space. Fig. 5(d) shows the profiles of pressure  $p$  and stresses  $T_z$  and  $t_z$  for each state labelled 1, 2 or 3 in Fig. 5(a).

For a uniform  $\tau_z$ , i.e. when  $\Delta\tau = 0$ , the axial stress is compressive in the epidermis and tensile in the core, with  $T_z(A) < 0 < T_z(0)$ , see case 1 in Fig. 5(a, d). This is purely a hydraulic effect due to the higher pressure at the surface,  $p(A) = p_a$ . As can be seen, this heterogeneity in stress and pressure becomes more visible when the radius  $A$  increases. When a gradient in wall extensibility is introduced, i.e. for  $\Delta\tau > 0$ , different scenarios are possible. For a relatively slender stem (i.e. above the dashed line), a state of epidermal tissue tension is observed, where both the total stress  $T_z$  and the partial solid stress  $t_z$  are maximal at the epidermis, see case 2 in Fig. 5(a, d). In this example, the core is in compression ( $T_z(0) < 0$ ); however, the solid matrix is generally still subject to tensile stresses ( $t_z(R) > 0$  for all  $R$ ), indicating that the cells remain turgid and that their walls

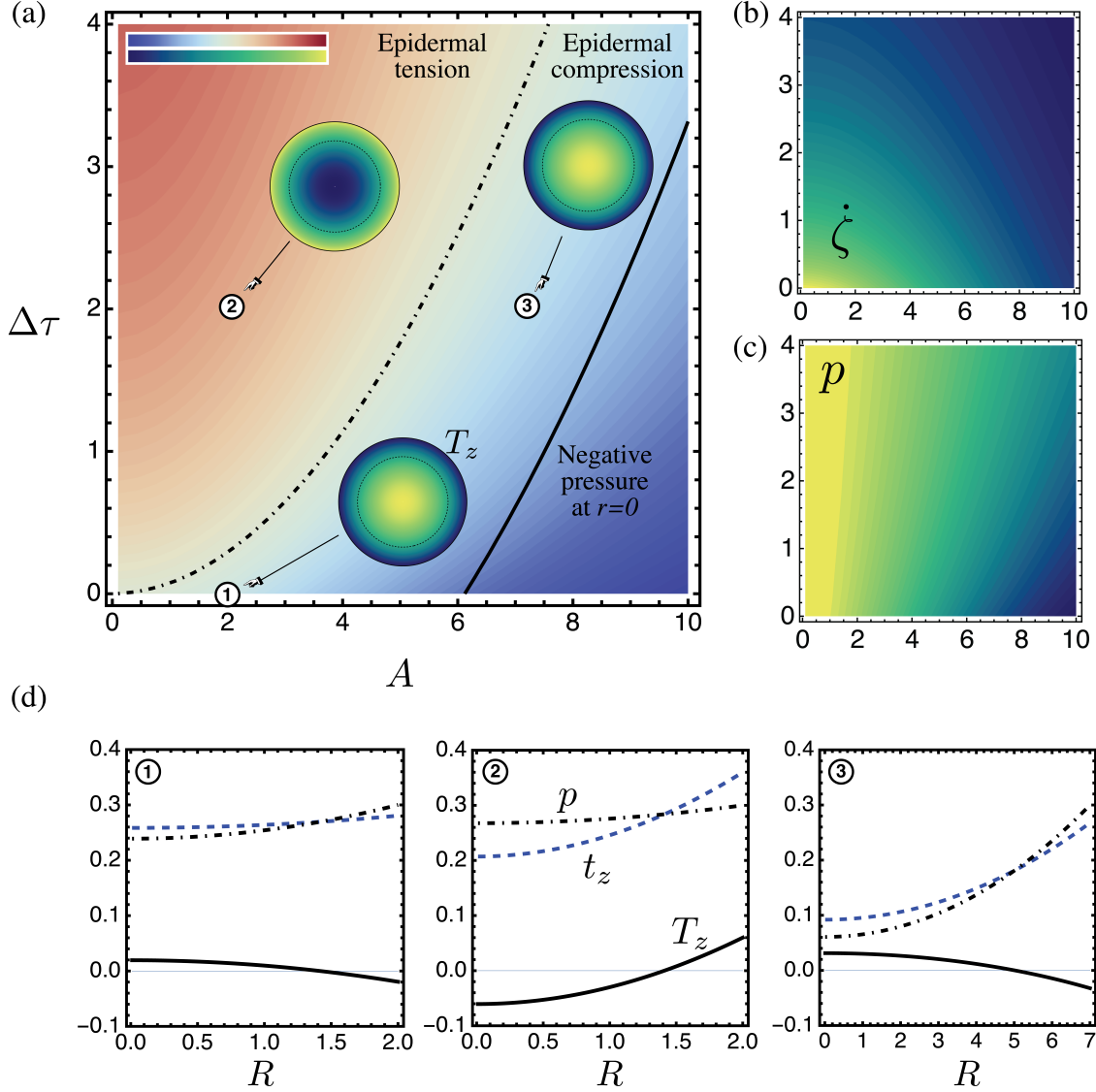


Figure 5: (a–c) Steady regime. (a) Contour plots shows differential tension  $\Delta T_z = T_z(A) - T_z(0)$  between the outside and the centre of the cylinder, plotted vs.  $A$  and  $\Delta\tau$ . Solid line indicate the points where a zone of negative pressure appears at the centre of the stem. Dot dashed line show the level set  $T_z(0) = T_z(A)$ ; above that line, the stress in the epidermis is higher than the stress at the centre. Insets show cross sections of the cylinder (scaled to the same radius) with colour indicating the axial stress  $T_z$  increasing from blue to yellow, with dashed line indicating level sets  $T_z = 0$ . (b) Rate of expansion  $\dot{\zeta}$  vs.  $A$  and  $\Delta\tau$ . (c) Mean pressure in the cross-section vs.  $A$  and  $\Delta\tau$ . (d) Axial stress profiles and pressure in the various scenarios 1, 2 and 3 of (a). Black solid line shows the total stress  $T_z = t_z - p$ ; Blue dashed line shows the partial stress  $t_z$ ; black dot-dashed line shows turgor pressure  $p$ . Parameters:  $p_a = 0.3$ ,  $\lambda = 1$ ,  $\alpha^* = 1$ .

are indeed under tension, despite the overall compressive stress. This observation challenges the conception that the cell walls should be compressed and possibly buckled due to overall tissue compression (as suggested in schematics by [Kutschera, 1989](#); [Peters and Tomos, 1996](#)). Overall, the distribution of stresses within a tissue is non trivial, in particular, the macroscopic stress—the one released upon cutting the tissue—is distinct from the stress experienced by the cell wall matrix.

For thicker stems, below the dashed line in Fig. 5(a), epidermal tension can no longer be maintained as hydraulic effects override the prescribed heterogeneity in extensibility. Indeed, as can be seen in Fig. 5(c, d), the pressure becomes low near the origin, indicating a water deficit due to the increased distance to the source, as is especially visible in case 3 in Fig. 5(a, d). As a result, a lower elongation rate  $\dot{\zeta}$  is observed; see Fig. 5(b). Here, even if the reduced epidermal extensibility would tend to promote epidermal tension, the epidermis is actually in compression, due to its better perfusion. A somewhat counterintuitive effect is observed where, unlike  $T_z$ , the axial stress  $t_z$  actually increases with  $R$ , i.e. the tension in the solid matrix is maximal in the epidermis notwithstanding the global compression. This effect can be interpreted in light of the heterogeneous pressure profile: While the epidermis has high turgor pressure, generating tension in the walls but overall compression within the tissue (since the epidermis is constrained by the core), the pressure near the origin is too low to generate much tension in the cell walls, and most part of the solid stress there is provided by the epidermis.

For even larger radii, i.e. below the solid line in Fig. 5(a), a central region appears where pressure at the origin is negative, i.e. the inequality (84) is violated. This extreme growth-induced effect results from the high deficit in water, and from axial tensile forces applied to the core by the epidermis, which effectively create a suction. While it is unclear whether such growth-induced negative pressure can exist, insofar as it results from the saturation assumption (10), we suspect that the relative water deficit within the core, and the associated tensile stresses, could potentially participate in cavity opening during stem hollowing, described mathematically by Goriely et al. (2010).

Following the developments of Section 2.6 we also assess the mechanical resistance of the stem under axial loads (i.e. its axial linear elastic modulus). We denote by  $\hat{\mathbf{A}} = \text{diag}(\hat{\alpha}_r, \hat{\alpha}_\theta, \hat{\alpha}_z)$  the incremental elastic deformation tensor, where  $\hat{\alpha}_r = \partial\hat{r}/\partial r$  and  $\hat{\alpha}_\theta = \hat{r}/r$ , with  $\hat{r}$  the radial coordinate in the incrementally deformed configuration. We first remark that the incompressibility condition  $(\hat{\alpha}_z\hat{r}/r)\partial\hat{r}/\partial r = 1$  is separable and can be integrated directly as  $\hat{r} = r/\sqrt{\hat{\alpha}_z}$  from which we obtain

$$\hat{\alpha}_r = \hat{\alpha}_\theta = 1/\sqrt{\hat{\alpha}_z}. \quad (85)$$

The stresses are given by (51) as

$$\hat{T}_i = t_i(\hat{\alpha}_r\alpha_r, \hat{\alpha}_\theta\alpha_\theta, \hat{\alpha}_z\alpha_z) - p - \hat{p}, \quad (86)$$

with  $i \in \{r, \theta, z\}$ . Taking the first variation of (85, 86) around the base solution  $\hat{\alpha}_i = 1$ , we derive

$$\delta\hat{T}_i = \mathcal{T}_i \delta\hat{\alpha}_z - \delta\hat{p}, \quad \text{with} \quad \mathcal{T}_i := \frac{\partial t_i}{\partial \alpha_z} - \frac{1}{2} \left( \frac{\partial t_i}{\partial \alpha_r} + \frac{\partial t_i}{\partial \alpha_\theta} \right). \quad (87)$$

Then, on integrating the balance of momentum

$$\frac{\partial(\delta\hat{T}_r)}{\partial r} = \frac{\mathcal{T}_\theta - \mathcal{T}_r}{r} \delta\hat{\alpha}_z, \quad (88)$$

and using the identity  $\delta\hat{T}_z - \delta\hat{T}_r = (\mathcal{T}_z - \mathcal{T}_r)\delta\hat{\alpha}_z$ , we obtain finally the total virtual reaction force of the whole stem

$$\delta F := 2\pi \int_0^a \delta T_z r dr = \mathcal{M}_z \delta\alpha_z, \quad (89)$$

with  $\mathcal{M}_z$  the effective longitudinal linear elasticity modulus given by

$$\mathcal{M}_z = 2\pi \int_0^a \left( \mathcal{T}_z - \mathcal{T}_r - \int_r^a \frac{\mathcal{T}_\theta - \mathcal{T}_r}{r'} dr' \right) r dr. \quad (90)$$

As can be seen,  $\mathcal{M}_z$  depends on the pre-existing stresses and stretches within the stem. In particular, in the absence of pre-stress ( $\alpha_r = \alpha_\theta = \alpha_z = 1$ ,  $p = 0$ ), we recover the known value  $\mathcal{M}_z^0 = 3\pi\mu B^2$  for the linear response of an incompressible neo-Hookean tube under uniaxial load. Fig. 6 shows the dependency of the relative stiffness  $\mathcal{M}_z/\mathcal{M}_z^0$  on  $A$  and  $\Delta\tau$ . As can be seen by comparing the level sets of Fig. 6 with those of Fig. 5(a), the variation in axial stiffness of the stem is related to the presence of axial residual stresses, measured by  $T_z(a) - T_z(0)$ . This observation supports the hypothesis that tissue tension confers higher rigidity to the stem (Kutschera, 2001; Sachs, 1882). However, unfortunately,  $\mathcal{K}_z$  does not inform us directly on the resistance of the stem to buckling, even for a thin stem, insofar as the residually-stressed cylinder is effectively heterogeneous and anisotropic. To that end, a full and likely tedious perturbation analysis including asymmetric modes is required (Gorieli et al., 2008b; Moulton et al., 2020; Vandiver and Gorieli, 2008).

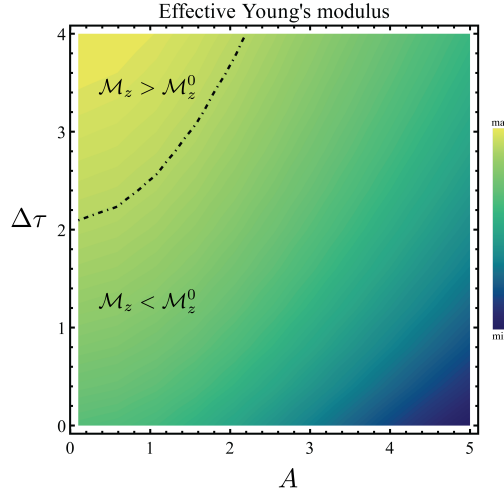


Figure 6: Apparent axial modulus  $\mathcal{M}_z$  of the residually-stressed stem in  $A$ - $\Delta\tau$  space. Dashed line indicate the locations in the parameter space where  $\mathcal{M}_z = \mathcal{M}_z^0$ , i.e. where the axial modulus is that of the unstressed stem of identical radius.

#### 4.3.2. Dynamic regime

These different states of the system can be observed in the full dynamic problem, as illustrated in Fig. 7. Here, we simulate the three-dimensional growth of a stem with  $\Delta\tau = 2$  taken as constant. To account for the rapid elongation of the stem, we also assume that the extensibility is smaller in the  $r$  and  $\theta$  directions ( $\tau_r = \tau_\theta = 10\tau_z$ , consistent with values used by Kelly-Bellow et al., 2023). As predicted earlier, epidermal tension is maintained until a critical radius is reached, at which point pressure becomes too low at the origin and epidermal compression appears. As the radius increases and the mean pressure decreases, the elongation rate  $\dot{\zeta}$  also decreases.

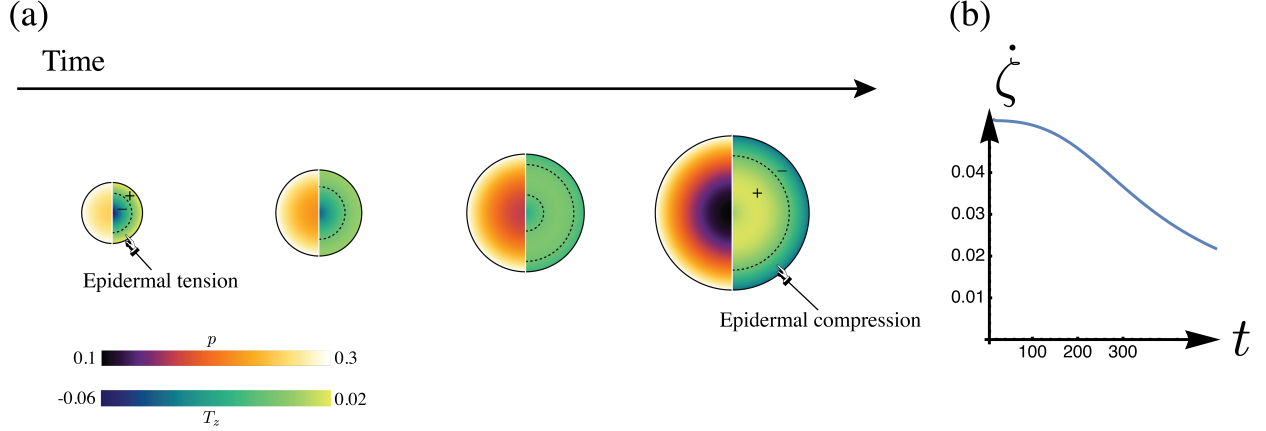


Figure 7: Dynamic regime. (a) Growing cross section of the stem for increasing time. The colour maps represent the turgor pressure  $p$  on the left (from dark to light); and the tensile stress on the right (from blue to yellow) with level set  $T_z = 0$  shown with dashed line. Initially, the stem is in a state of epidermal tension due to positive  $\Delta\tau$ . Later on, pressure decreases in the core and epidermal tension vanishes. (b) Relative elongation rate  $\dot{\zeta}$  vs. time. Parameters:  $\Delta\tau = 1$ ,  $p_a = 0.3$ ,  $\lambda = 1$ ,  $\alpha^* = 1$ ,  $A = 1$ .

## 5. Growth of a sphere

As a final example, we study the full model (46) including the transport of osmolytes, that is, instead of assuming a constant osmotic pressure as in Sections 3, 4, we here assume that the osmolytes can diffuse on the growing domain, here a thick spherical shell. This example illustrates how physiochemical details of organ growth can be included, for instance in the context of fruit growth which involves complex transport of sugar, gas exchanges and water fluxes. Although we do not aim here to model the sheer physiological complexity of fruit growth and maturation, our approach provides a paradigm to generalise detailed zero-dimensional multi-compartment approaches—e.g. Bussières (1994); Cieslak et al. (2016); Dequeker et al. (2024); Fishman and Génard (1998); Martre et al. (2011)—to a continuum.

We study the growth of a hollow sphere of inner and outer radius  $a$  and  $b$  in the current configuration ( $A$  and  $B$  respectively in the reference configuration). We introduce the system of spherical coordinates  $(r, \theta, \varphi)$  in current configuration and  $(R, \Theta, \Phi)$  in reference configuration; see Fig. 8(a). We assume the problem to be spherically symmetric so that, as in Section 4, the problem only involves the coordinates  $r$  and  $t$ .

For simplicity, we neglect active transport of the osmolytes ( $\bar{\mathbf{f}}_o = 0$ ) and we write  $\mathbf{L}_{os} = (c_o R_g \theta / D_{os}) \mathbf{1}$  with  $D_{os}$  the diffusivity of the osmolytes in the solid, so that (41) can be written as a standard Fickian flux  $\mathbf{j}_o = -D_{os} \nu_o \partial c_o / \partial r \mathbf{e}_r$ . We assume that the outer hydrostatic pressure is zero on both faces of the shell. For the flux of material, we assume a Dirichlet condition (48) at  $r = a$ . At the outer boundary  $r = b$ , we postulate an transpiration outflux associated with a water potential  $\psi_{ev}$  and conductivity  $k_b$ . Altogether, we have

$$\begin{aligned}
 t_r(a, t) &= p(a, t), & \pi(a, t) &= \pi_a; & \psi(a, t) &= \psi_a, \\
 t_r(b, t) &= p(b, t), & \frac{\partial \psi}{\partial r}(b, t) &= k_b(\psi_{ev} - \psi), & \frac{\partial \pi}{\partial r}(b, t) &= 0,
 \end{aligned} \tag{91}$$

with  $\psi_a$  the water potential across the inner boundary; and  $\pi_a$  the osmotic pressure at  $r = a$ . We assume  $\xi_f = \xi_o = 0$ , so that the only source of water and osmolyte mass is the inner boundary. Following a procedure similar to that of [Section 4](#), we derive the (nondimensionalised) governing equations for the growing sphere:

$$\frac{\partial t_r}{\partial r} + \frac{2}{r}(t_r - t_\theta) = \frac{\partial p}{\partial r}, \quad (92a)$$

$$v - \frac{\partial}{\partial r}(p - \pi) = \frac{b^2}{r^2}(\dot{b} - k_b(\psi_{ev} - p_b + \pi_b)), \quad (92b)$$

$$v\pi - D_{os}v_o \frac{\partial \pi}{\partial r} = \frac{b^2 \dot{b} \pi_b}{r^2}, \quad (92c)$$

$$\frac{\dot{\gamma}_r}{\gamma_r} = \frac{1}{2}(\alpha_r^2 - \alpha^{*2})_+, \quad \frac{\dot{\alpha}_r}{\alpha_r} + \frac{1}{2}(\alpha_r^2 - \alpha^{*2})_+ = \frac{\partial v}{\partial r}, \quad \frac{\dot{\alpha}_\theta}{\alpha_\theta} + \frac{1}{2}(\alpha_\theta^2 - \alpha^{*2})_+ = \frac{v}{r}, \quad (92d)$$

$$t_r = \frac{1}{\alpha_\theta^2} \frac{\partial \Psi_s}{\partial \alpha_r}, \quad t_\theta = \frac{1}{\alpha_r \alpha_\theta} \frac{\partial \Psi_s}{\partial \alpha_\theta}, \quad (92e)$$

where we have used the approximated van 't Hoff relation  $\pi \approx R\theta\phi_o/v_o$ , the two no-flux boundary conditions (91) to integrate (46a, 46b), and the neo-Hookean strain energy (81); and where  $\pi_b := \pi(b)$  and  $p_b := p(b)$  are the undetermined osmotic and hydrostatic pressures at the outer boundary. We have assumed that the osmolyte diffusion is fast and in the quasi-steady regime, so that we set  $\partial\phi_o/\partial t = 0$  in (46b). All parameters are taken to be uniform across the domain and constant in time. [Fig. 8\(b\)](#) illustrates the evolution of pressure in a typical simulation. We see that during growth, the pressure drops in regions located far from the central source (similar to [Section 4](#)). This simulation illustrates again the dynamic nature of pressure in the context of growth and osmotic regulations with multiple interfaces. This approach may be beneficial to integrate spatiotemporal details of physiological and mechanical regulations in fruit development, as well as nonlocal couplings, which cannot be captured using more basic zero-dimensional models.

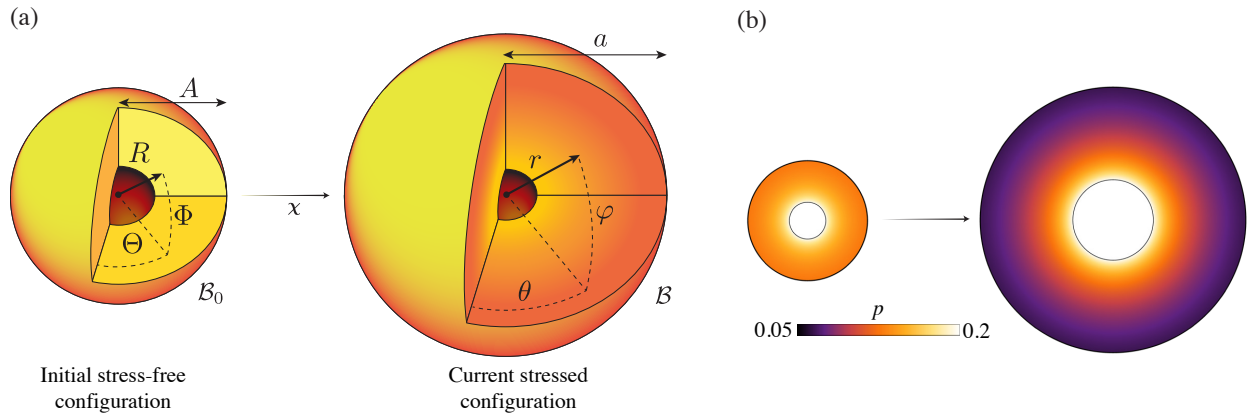


Figure 8: Growth of a hollow sphere. (a) Geometry: initial and current configuration with associated spherical coordinate systems. (b) Example simulation showing a drop in outer pressure during growth. Parameters:  $A = 0.03$ ,  $B = 0.1$ ,  $\pi_a = 0.2$ ,  $k_b = 0.5$ ,  $\Psi_{ev} = 0$ ,  $\alpha^* = 1$ ,  $\lambda = 1$ ,  $D_{os}v_o = 1$ .



## 6. Discussion

While many continuum models of plant tissues morphogenesis have relied on phenomenological kinematic specifications of the growth behaviour, the establishment of a mechanistic theory of morphogenesis requires modelling growth in relation to more fundamental physical and mechanical fields (Ambrosi et al., 2011, 2019; Goriely, 2017; Kuhl, 2014; Menzel and Kuhl, 2012). In plants, it is widely accepted that cellular growth results from mechanical deformations of the cell walls driven by cell osmolarity. However, the explicit connection between pressure and growth has not been systematically integrated in continuum models. To bridge this gap, we proposed a formulation of plant developmental processes that extends the paradigm of Lockhart, Cosgrove and Ortega to a hydromechanical continuum description of the growth phenomenon.

The role of pressure have been considered in numerous multicellular discrete models which have described growth as a result of turgor-induced cell wall expansion. However, typically, these models have treated pressure as a prescribed biological parameter, thereby neglecting the fundamentally mechanical nature of pressure. Physically, this modelling simplification originates in the assumption that growth is primarily limited by the cell wall extensibility  $\Phi$ , thus, that water exchanges across cell membranes are instantaneous (i.e.  $p \approx \pi$ ). While this assumption may hold true in a first approximation, such simplification does not allow for a complete representation of the physical events occurring during growth. Recent reevaluation of water conductivity contributions in various systems has also revealed a nuanced role of hydraulic effects, which may be non-negligible (Alonso-Serra et al., 2024; Laplaud et al., 2024; Long et al., 2020). These advancements motivate the development of new models based on a proper formulation of turgor. Indeed, the fundamental interplay between pressure, fluxes, osmolarity and cell mechanics is critical for a proper understanding of the notion of turgor, with profound experimental and conceptual implications. Thus, we assert that a robust physical description of growth should be grounded in clear balance relations. Our poroelastic theory captures the growth of a tissue as the result of simultaneous mechanically-induced cell wall expansion and water fluxes. Thus, pressure is treated as a dependent mechanical variable that mediates the growth deformations indirectly, through the balance of forces. This integrated perspective is directly in line with the original philosophy of Lockhart’s approach.

A key mass balance principle can be stated as follows: For growth to occur, water must flow to fill the expanding volume, irrespective of the cause of cell wall expansion. In other words, growing regions correspond to hydraulic sinks and fast-growing regions are associated with lower water potential, as exemplified in Section 3. Such sink is characterised by the development of growth-induced gradients of water potential and a water flux directed towards the growing region, an idea which has surfaced in the literature in particular in the work of Boyer and coworkers (Boyer, 1988; Boyer et al., 1985; Molz and Boyer, 1978; Nonami and Boyer, 1993; Passioura and Boyer, 2003). This flux, captured here through a Darcy-type law (44), introduces a fundamental growth-induced *hydromechanical length*  $\mathcal{L}_h = \sqrt{KE\tau_0}$  which reflects the combined effects of growth ( $\tau$ ), tissue permeability ( $K$ ), and elasticity ( $E$ ). For growing avascular domains larger than this typical length, interesting nonlocal couplings may emerge. For example, in Section 3.2, we predicted that a fast growing region will absorb water from its neighbourhood, thereby hindering its growth. This idea is reminiscent of patterning mechanisms based on lateral inhibition (Meinhardt and Gierer, 2000).



Such phenomenon has been predicted in previous theoretical study (Cheddadi et al., 2019) and was recently observed experimentally in *Arabidopsis thaliana* shoot apices, where peripheral cells adjacent to incipient organs exhibit a shrinkage consistent with a water deficit (Alonso-Serra et al., 2024). Here we characterise mathematically the magnitude and spatial extent of this inhibition (Fig. 2). In particular, we show that inhibition will be amplified and more spatially extended in weakly vascularised tissues ( $k \ll 1$ ), where the inhibition zone is expected to have a width  $\sim \mathcal{L}_h$ .

The role of hydromechanical effects is also illustrated in three dimensions in our model of a growing stem. Firstly, we showed that the classic epidermal tension hypothesis could be naturally captured by a gradient in cell extensibility; reproducing the phenomenology of previous continuum models (Goriely et al., 2010; Kelly-Bellow et al., 2023). Secondly, for thick stems where the distance to the vascular bundle increases, the distribution of residual stresses was greatly perturbed by hydraulic scaling effects when pressure at the core became very low. Naturally, in reality, the vascular architecture of plants may evolve as part of the developmental process to maintain adequate vascularisation. Therefore, we anticipate that our predictions may not apply universally, and the model must be adapted to capture more realistic scenarios. Overall, this work aims to exhibit guiding principles of hydromechanical control of plant morphogenesis and illustrate the complex, nonlocal and fundamentally dynamic behaviours that emerge from integrating fundamental growth mechanisms in space and time.

Several questions remain open. The most pressing problem is to formulate a constitutive law describing growth, specifically the process by which the cell walls expand and solid mass is added to the system. Although a strain-based growth law could capture the basic phenomenology of plant growth, its mechanistic interpretation is not fully established, in particular, it remains unclear which specific mechanical quantity should be adopted as a driver of growth, and whether an appropriate growth law can be derived from rational mechanics considerations (Section 2.3.2). Furthermore, a realistic growth law should also be able to capture the multiscale link between local cell structures and anisotropies and the overall growth of the tissue at the continuum level. In this context, promising efforts to derive continuum representations from the cellular structures using multiscale analysis are emerging (Boudaoud et al., 2023), and we hope that our work will motivate further advances in this area.

Another question concerns the link between the effective permeability tensor and the microscopic details of water routes within the tissue. In the context of direct cell-to-cell water transport (Cheddadi et al., 2019), an approach would consist of deriving the effective hydraulic conductivity of a periodically-repeating representative cell network using two-scale analysis, as described by Chapman and Shabala (2017). More in general, the biological details of water transport in different tissues are still an active subject of research, thus the precise biophysical interpretation of the effective conductivity is yet to be better characterised. For example, an interesting extension to our model would be to treat the apoplasmic route and the transmembrane exchanges between cell vacuoles separately (Molz and Ikenberry, 1974).

Lastly, a natural extension to this work is to model the role of morphogens (e.g. hormones, such as auxin, or genes), using regular advection-diffusion equations, or more complex, nonlinear reaction-diffusion-advection-systems (Kennaway and Coen, 2019; Kierzkowski et al., 2019; Krause et al., 2023; Moulton et al., 2020; Newell et al., 2008; Rueda-Contreras et al., 2018). In the

spirit of our approach, these morphogens should regulate specific physical and mechanical properties of the system, such as the rigidity, the osmolarity, the growth threshold or the cell extensibility, thereby indirectly influencing growth.

Overall, this work lays the foundations of a field theory of plant morphogenesis—a closed mathematical framework in which the growth phenomenon emerges as the product of multiple, coupled physical, chemical and mechanical fields acting more or less nonlocally. The construction of such theories is a formidable challenge in plant biomechanics and, in general, in the study of active living materials. In this broader context, the unassuming plant provides an interesting paradigm to build a general theory of living tissues.

## Acknowledgement

I.C. acknowledges support from the *Institut rhônalpin des systèmes complexes (IXXI)*, and the *Agence Nationale pour la Recherche* through the research project *HydroField*. The authors are grateful to Alain Goriely, Andrea Giudici, Christophe Godin, and Arezki Boudaoud for insightful discussions.

## Appendix A. Numerics and implementation

We integrate the system using a relaxation method (backward time, centred space); see [Press et al. \(2007\)](#). All simulations were implemented in the software *Wolfram Mathematica 14.0*. Source code is available upon request.

## References

- Ali, O., Cheddadi, I., Landrein, B., and Long, Y. (2023). Revisiting the relationship between turgor pressure and plant cell growth. *New Phytologist*, 238(1):62–69.
- Ali, O., Mirabet, V., Godin, C., and Traas, J. (2014). Physical models of plant development. *Annual Review of Cell and Developmental Biology*, 30(1):59–78.
- Ali, O., Oliveri, H., Traas, J., and Godin, C. (2019). Simulating turgor-induced stress patterns in multilayered plant tissues. *Bulletin of Mathematical Biology*, 81(8):3362–3384.
- Ali, O. and Traas, J. (2016). Force-Driven Polymerization and Turgor-Induced Wall Expansion. *Trends in Plant Science*, 21(5):398–409.
- Alim, K., Hamant, O., and Boudaoud, A. (2012). Regulatory role of cell division rules on tissue growth heterogeneity. *Frontiers in Plant Science*, 3:174.
- Alonso-Serra, J., Cheddadi, I., Kiss, A., Cerutti, G., Lang, M., Dieudonné, S., Lionnet, C., Godin, C., and Hamant, O. (2024). Water fluxes pattern growth and identity in shoot meristems. *Nature Communications*, 15(1):1–14.

- Ambrosi, D., Ateshian, G. A., Arruda, E. M., Cowin, S. C., Dumais, J., Goriely, A., Holzapfel, G. A., Humphrey, J. D., Kemkemer, R., Kuhl, E., Olberding, J. E., Taber, L. A., and Garikipati, K. R. (2011). Perspectives on biological growth and remodeling. *Journal of the Mechanics and Physics of Solids*, 59(4):863–883.
- Ambrosi, D., Ben Amar, M., Cyron, C. J., DeSimone, A., Goriely, A., Humphrey, J. D., and Kuhl, E. (2019). Growth and remodelling of living tissues: perspectives, challenges and opportunities. *Journal of the Royal Society Interface*, 16(157):20190233.
- Ambrosi, D. and Guana, F. (2007). Stress-modulated growth. *Mathematics and mechanics of solids*, 12(3):319–342.
- Ambrosi, D., Preziosi, L., and Vitale, G. (2012). The interplay between stress and growth in solid tumors. *Mechanics Research Communications*, 42:87–91.
- Barbacci, A., Lahaye, M., and Magnenet, V. (2013). Another brick in the cell wall: biosynthesis dependent growth model. *PLoS One*, 8(9):e74400.
- Bassel, G. W., Stamm, P., Mosca, G., Barbier de Reuille, P., Gibbs, D. J., Winter, R., Janka, A., Holdsworth, M. J., and Smith, R. S. (2014). Mechanical constraints imposed by 3D cellular geometry and arrangement modulate growth patterns in the Arabidopsis embryo. *Proceedings of the National Academy of Sciences*, page 201404616.
- Bedford, A. and Drumheller, D. S. (1983). Theories of immiscible and structured mixtures. *International Journal of Engineering Science*, 21(8):863–960.
- Ben Amar, M. and Goriely, A. (2005). Growth and instability in elastic tissues. *Journal of the Mechanics and Physics of Solids*, 53:2284–2319.
- Bessonov, N., Mironova, V., and Volpert, V. (2013). Deformable cell model and its application to growth of plant meristem. *Mathematical Modelling of Natural Phenomena*, 8(4):62–79.
- Bou Daher, F., Chen, Y., Bozorg, B., Clough, J., Jönsson, H., and Braybrook, S. A. (2018). Anisotropic growth is achieved through the additive mechanical effect of material anisotropy and elastic asymmetry. *eLife*, 7:e38161.
- Boudaoud, A. (2010). An introduction to the mechanics of morphogenesis for plant biologists. *Trends in plant science*, 15(6):353–360.
- Boudaoud, A., Kiss, A., and Ptashnyk, M. (2023). Multiscale modeling and analysis of growth of plant tissues. *SIAM Journal on Applied Mathematics*, 83(6):2354–2389.
- Boudon, F., Chopard, J., Ali, O., Gilles, B., Hamant, O., Boudaoud, A., Traas, J., and Godin, C. (2015). A Computational Framework for 3D Mechanical Modeling of Plant Morphogenesis with Cellular Resolution. *PLoS Computational Biology*, 11(1):e1003950.

- Boyer, J. S. (1988). Cell enlargement and growth-induced water potentials. *Physiologia Plantarum*, 73(2):311–316.
- Boyer, J. S., Cavalieri, A., and Schulze, E. D. (1985). Control of the rate of cell enlargement: excision, wall relaxation, and growth-induced water potentials. *Planta*, 163:527–543.
- Bozorg, B., Krupinski, P., and Jönsson, H. (2016). A continuous growth model for plant tissue. *Physical Biology*, 13(6):065002.
- Bussièrès, P. (1994). Water Import Rate in Tomato Fruit: A Resistance Model. *Annals of Botany*, 73(1):75–82.
- Chakraborty, J., Luo, J., and Dyson, R. J. (2021). Lockhart with a twist: Modelling cellulose microfibril deposition and reorientation reveals twisting plant cell growth mechanisms. *Journal of Theoretical Biology*, 525:110736.
- Chapman, S. J. and Shabala, A. (2017). Effective transport properties of lattices. *SIAM Journal on Applied Mathematics*, 77(5):1631–1652.
- Cheddadi, I., Génard, M., Bertin, N., and Godin, C. (2019). Coupling water fluxes with cell wall mechanics in a multicellular model of plant development. *PLoS Computational Biology*, 15(6):e1007121.
- Chickarmane, V., Roeder, A. H., Tarr, P. T., Cunha, A., Tobin, C., and Meyerowitz, E. M. (2010). Computational morphodynamics: a modeling framework to understand plant growth. *Annual review of plant biology*, 61:65–87.
- Cieslak, M., Cheddadi, I., Boudon, F., Baldazzi, V., Génard, M., Godin, C., and Bertin, N. (2016). Integrating physiology and architecture in models of fruit expansion. *Frontiers in plant science*, 7:1739.
- Coen, E. (1999). *The art of genes: How organisms make themselves*. Oxford University Press, Oxford.
- Coen, E. and Cosgrove, D. J. (2023). The mechanics of plant morphogenesis. *Science*, 379(6631):eade8055.
- Coen, E., Kennaway, R., and Whitewoods, C. (2017). On genes and form. *Development*, 144(23):4203–4213.
- Coen, E., Rolland-Lagan, A.-G., Matthews, M., Bangham, J. A., and Prusinkiewicz, P. (2004). The genetics of geometry. *Proceedings of the National Academy of Sciences of the United States of America*, 101(14):4728–4735.
- Coleman, B. D. and Noll, W. (1963). The thermodynamics of elastic materials with heat conduction and viscosity. *Archive for Rational Mechanics and Analysis*, 13(1):167 – 178.

- Corson, F., Hamant, O., Bohn, S., Traas, J., Boudaoud, A., and Couder, Y. (2009). Turning a plant tissue into a living cell froth through isotropic growth. *Proceedings of the National Academy of Sciences*, 106(21):8453–8458.
- Cosgrove, D. J. (1981). Analysis of the dynamic and steady-state responses of growth rate and turgor pressure to changes in cell parameters. *Plant Physiology*, 68(6):1439–1446.
- Cosgrove, D. J. (1985). Cell wall yield properties of growing tissue: evaluation by in vivo stress relaxation. *Plant physiology*, 78(2):347–356.
- Cosgrove, D. J. (1993). Water uptake by growing cells: an assessment of the controlling roles of wall relaxation, solute uptake, and hydraulic conductance. *International journal of plant sciences*, 154(1):10–21.
- Cosgrove, D. J. (2005). Growth of the plant cell wall. *Nature reviews molecular cell biology*, 6(11):850–861.
- Cosgrove, D. J. (2016). Plant cell wall extensibility: connecting plant cell growth with cell wall structure, mechanics, and the action of wall-modifying enzymes. *Journal of experimental botany*, 67(2):463–476.
- Cosgrove, D. J. (2018). Diffuse growth of plant cell walls. *Plant physiology*, 176(1):16–27.
- Cosgrove, D. J. and Anderson, C. T. (2020). Plant cell growth: do pectins drive lobe formation in Arabidopsis pavement cells? *Current Biology*, 30(11):R660–R662.
- Coussy, O. (2003). *Poromechanics*. John Wiley & Sons, Chichester.
- Curtis, C. C. (1914). *Nature and development of plants*. Henry Holt and Company, New York, 4 edition.
- Dainty, J. (1963). Water relations of plant cells. In Preston, R. D., editor, *Volume 1, Advances in Botanical Research*, pages 279–326. Academic Press.
- De Boer, R. (1992). Development of porous media theories—a brief historical review. *Transport in porous media*, 9:155–164.
- De Boer, R. (2012). *Theory of porous media: highlights in historical development and current state*. Springer Berlin, Heidelberg.
- Dequeker, B., Šalagovič, J., Retta, M., Verboven, P., and Nicolai, B. M. (2024). A biophysical model of apple (*Malus domestica* Borkh.) and pear (*Pyrus communis* L.) fruit growth. *Biosystems Engineering*, 239:130–146.
- Dervaux, J. and Ben Amar, M. (2008). Morphogenesis of growing soft tissues. *Physical Review Letters*, 101:068101.

- DiCarlo, A. and Quiligotti, S. (2002). Growth and balance. *Mechanics Research Communications*, 29(6):449–456.
- Dumais, J. (2021). Mechanics and hydraulics of pollen tube growth. *New Phytologist*, 232(4):1549–1565.
- Dumais, J. and Forterre, Y. (2012). “Vegetable dynamicks”: the role of water in plant movements. *Annual Review of Fluid Mechanics*, 44:453–478.
- Dunlop, J. W., Fischer, F. D., Gamsjäger, E., and Fratzl, P. (2010). A theoretical model for tissue growth in confined geometries. *Journal of the Mechanics and Physics of Solids*, 58(8):1073–1087.
- Dupuy, L., Mackenzie, J., Rudge, T., and Haseloff, J. (2007). A system for modelling cell-cell interactions during plant morphogenesis. *Annals of botany*, 101(8):1255–1265.
- Dyson, R. J., Band, L. R., and Jensen, O. E. (2012). A model of crosslink kinetics in the expanding plant cell wall: Yield stress and enzyme action. *Journal of Theoretical Biology*, 307:125–136.
- Eggen, E., de Keijzer, M. N., and Mulder, B. M. (2011). Self-regulation in tip-growth: The role of cell wall ageing. *Journal of theoretical biology*, 283(1):113–121.
- Epstein, M. and Maugin, G. A. (2000). Thermomechanics of volumetric growth in uniform bodies. *International Journal of Plasticity*, 16(7-8):951–978.
- Erickson, R. O. (1976). Modeling of plant growth. *Annual review of plant physiology*, 27(1):407–434.
- Fishman, S. and Génard, M. (1998). A biophysical model of fruit growth: simulation of seasonal and diurnal dynamics of mass. *Plant, Cell & Environment*, 21(8):739–752.
- Forterre, Y. (2013). Slow, fast and furious: understanding the physics of plant movements. *Journal of experimental botany*, 64(15):4745–4760.
- Forterre, Y. (2022). Basic soft matter for plants. In Jensen, K. and Forterre, Y., editors, *Soft Matter in Plants: From Biophysics to Biomimetics*, number 15 in Soft Matter Series, chapter 1, pages 1–65. The Royal Society of Chemistry, London.
- Fozard, J. A., Lucas, M., King, J. R., and Jensen, O. E. (2013). Vertex-element models for anisotropic growth of elongated plant organs. *Frontiers in Plant Science*, 4(233).
- Fraldi, M. and Carotenuto, A. R. (2018). Cells competition in tumor growth poroelasticity. *Journal of the Mechanics and Physics of Solids*, 112:345–367.
- Fridman, Y., Strauss, S., Horev, G., Ackerman-Lavert, M., Reiner-Benaim, A., Lane, B., Smith, R., and Savaldi-Goldstein, S. (2021). The root meristem is shaped by brassinosteroid control of cell geometry. *Nature plants*, 7(11):1475–1484.

- Geitmann, A. and Ortega, J. K. E. (2009). Mechanics and modeling of plant cell growth. *Trends in Plant Science*, 14(9):467–478.
- Goriely, A. (2017). *The mathematics and mechanics of biological growth*, volume 45 of *Interdisciplinary applied mathematics*. Springer-Verlag, New York.
- Goriely, A., Moulton, D. E., and Vandiver, R. (2010). Elastic cavitation, tube hollowing, and differential growth in plants and biological tissues. *Europhysics Letters*, 91(1):18001.
- Goriely, A., Robertson-Tessi, M., Tabor, M., and Vandiver, R. (2008a). Elastic growth models. In Mondaini, R. P. and Pardalos, P. M., editors, *Mathematical modelling of biosystems*, volume 102 of *Applied Optimization*, chapter 1, pages 1–44. Springer-Verlag Berlin Heidelberg.
- Goriely, A. and Tabor, M. (1998). Spontaneous helix hand reversal and tendril perversion in climbing plants. *Physical Review Letters*, 80:1564–1567.
- Goriely, A., Vandiver, R., and Destrade, M. (2008b). Nonlinear Euler buckling. *Proceedings of the Royal Society A: Mathematical, Physical and Engineering Sciences*, 464(2099):3003–3019.
- Green, A. A., Kennaway, J. R., Hanna, A. I., Bangham, J. A., and Coen, E. (2010). Genetic Control of Organ Shape and Tissue Polarity. *PLoS Computational Biology Biol*, 8(11):e1000537.
- Gurtin, M. E., Fried, E., and Anand, L. (2010). *The mechanics and thermodynamics of continua*. Cambridge University Press, New York.
- Haas, K. T., Wightman, R., Meyerowitz, E. M., and Peaucelle, A. (2020). Pectin homogalacturonan nanofilament expansion drives morphogenesis in plant epidermal cells. *Science*, 367(6481):1003–1007.
- Haas, K. T., Wightman, R., Peaucelle, A., and Höfte, H. (2021). The role of pectin phase separation in plant cell wall assembly and growth. *The Cell Surface*, 7:100054.
- Hamant, O., Heisler, M. G., Jonsson, H., Krupinski, P., Uyttewaal, M., Bokov, P., Corson, F., Sahlín, P., Boudaoud, A., Meyerowitz, E. M., Couder, Y., and Traas, J. (2008). Developmental patterning by mechanical signals in Arabidopsis. *Science*, 322(5908):1650–1655.
- Hamant, O. and Traas, J. (2010). The mechanics behind plant development. *New Phytologist*, 185(2):369–385.
- Holland, M. A., Kosmata, T., Goriely, A., and Kuhl, E. (2013). On the mechanics of thin films and growing surfaces. *Mathematics and Mechanics of Solids*, 18(6):561–575.
- Holzappel, G. A. (2000). *Nonlinear solid mechanics*. John Wiley & Sons, Chichester.
- Jia, F., Pearce, S. P., and Goriely, A. (2018). Curvature delays growth-induced wrinkling. *Physical Review E*, 98(3):033003.



- Johnson, K. and Lenhard, M. (2011). Genetic control of plant organ growth. *New Phytologist*, 191(2):319–333.
- Kelly-Bellow, R., Lee, K., Kennaway, R., Barclay, J. E., Whibley, A., Bushell, C., Spooner, J., Yu, M., Brett, P., Kular, B., Cheng, S., Chu, J., Xu, T., Lane, B., Fitzsimons, J., Xue, Y., Smith, R. S., Whitewoods, C. D., and Coen, E. (2023). Brassinosteroid coordinates cell layer interactions in plants via cell wall and tissue mechanics. *Science*, 380(6651):1275–1281.
- Kennaway, R. and Coen, E. (2019). Volumetric finite-element modelling of biological growth. *Open biology*, 9(5):190057.
- Kennaway, R., Coen, E., Green, A., and Bangham, A. (2011). Generation of Diverse Biological Forms through Combinatorial Interactions between Tissue Polarity and Growth. *PLoS Computational Biology*, 7(6):e1002071.
- Khadka, J., Julien, J.-D., and Alim, K. (2019). Feedback from tissue mechanics self-organizes efficient outgrowth of plant organ. *Biophysical journal*, 117(10):1995–2004.
- Kierzkowski, D., Nakayama, N., Routier-Kierzkowska, A.-L., Weber, A., Bayer, E., Schorderet, M., Reinhardt, D., Kuhlemeier, C., and Smith, R. S. (2012). Elastic domains regulate growth and organogenesis in the plant shoot apical meristem. *Science*, 335(6072):1096–1099.
- Kierzkowski, D., Runions, A., Vuolo, F., Strauss, S., Lymbouridou, R., Routier-Kierzkowska, A.-L., Wilson-Sánchez, D., Jenke, H., Galinha, C., Mosca, G., et al. (2019). A growth-based framework for leaf shape development and diversity. *Cell*, 177(6):1405–1418.
- Krause, A. L., Gaffney, E. A., and Walker, B. J. (2023). Concentration-dependent domain evolution in reaction–diffusion systems. *Bulletin of Mathematical Biology*, 85(2):14.
- Kuhl, E. (2014). Growing matter: A review of growth in living systems. *Journal of the Mechanical Behavior of Biomedical Materials*, 29:529–543.
- Kutschera, U. (1989). Tissue stresses in growing plant organs. *Physiologia Plantarum*, 77(1):157–163.
- Kutschera, U. (2001). Gravitropism of axial organs in multicellular plants. *Advances in Space Research*, 27(5):851–860.
- Kutschera, U., Bergfeld, R., and Schopfer, P. (1987). Cooperation of epidermis and inner tissues in auxin-mediated growth of maize coleoptiles. *Planta*, 170(2):168–180.
- Kutschera, U. and Niklas, K. J. (2007). The epidermal-growth-control theory of stem elongation: An old and a new perspective. *Journal of Plant Physiology*, 164(11):1395–1409.
- Lang, G. E., Vella, D., Waters, S. L., and Goriely, A. (2015). Propagation of damage in brain tissue: coupling the mechanics of oedema and oxygen delivery. *Biomechanics and modeling in mechanobiology*, 14:1197–1216.

- Laplaud, V., Muller, E., Demidova, N., Drevensek, S., and Boudaoud, A. (2024). Assessing the hydromechanical control of plant growth. *Journal of the Royal Society Interface*, 21(214):20240008.
- Lee, K. J. I., Bushell, C., Koide, Y., Fozard, J. A., Piao, C., Yu, M., Newman, J., Whitewoods, C., Avondo, J., Kennaway, R., Marée, A. F. M., Cui, M., and Coen, E. (2019). Shaping of a three-dimensional carnivorous trap through modulation of a planar growth mechanism. *PLoS Biology*, 17(10):e3000427.
- Liang, H. and Mahadevan, L. (2009). The shape of a long leaf. *Proceedings of the National Academy of Sciences*, 106(52):22049–22054.
- Liu, S., Strauss, S., Adibi, M., Mosca, G., Yoshida, S., Dello Ioio, R., Runions, A., Andersen, T. G., Grossmann, G., Huijser, P., Smith, R. S., and Tsiantis, M. (2022). Cytokinin promotes growth cessation in the Arabidopsis root. *Current Biology*, 32(9):1974–1985.e3.
- Liu, Z., Swaddiwudhipong, S., and Hong, W. (2013). Pattern formation in plants via instability theory of hydrogels. *Soft Matter*, 9(2):577–587.
- Lockhart, J. A. (1965). An analysis of irreversible plant cell elongation. *Journal of theoretical biology*, 8(2):264–275.
- Long, Y., Cheddadi, I., Mosca, G., Mirabet, V., Dumond, M., Kiss, A., Traas, J., Godin, C., and Boudaoud, A. (2020). Cellular heterogeneity in pressure and growth emerges from tissue topology and geometry. *Current Biology*, 30(8):1504–1516.
- Martre, P., Bertin, N., Salon, C., and Génard, M. (2011). Modelling the size and composition of fruit, grain and seed by process-based simulation models. *New Phytologist*, 191(3):601–618.
- Martyushev, L. M. and Seleznev, V. D. (2006). Maximum entropy production principle in physics, chemistry and biology. *Physics reports*, 426(1):1–45.
- Meinhardt, H. and Gierer, A. (2000). Pattern formation by local self-activation and lateral inhibition. *BioEssays*, 22(8):753–760.
- Menzel, A. and Kuhl, E. (2012). Frontiers in growth and remodeling. *Mechanics research communications*, 42:1–14.
- Merks, R. M., Guravage, M., Inzé, D., and Beemster, G. T. (2011). VirtualLeaf: an open-source framework for cell-based modeling of plant tissue growth and development. *Plant physiology*, 155(2):656–666.
- Molz, F. J. and Boyer, J. S. (1978). Growth-induced water potentials in plant cells and tissues. *Plant Physiology*, 62(3):423–429.
- Molz, F. J. and Ikenberry, E. (1974). Water transport through plant cells and cell walls: theoretical development. *Soil Science Society of America Journal*, 38(5):699–704.

- Molz, F. J., Truelove, B., and Peterson, C. M. (1975). Dynamics of rehydration in leaf disks 1. *Agronomy Journal*, 67(4):511–515.
- Mosca, G., Adibi, M., Strauss, S., Runions, A., Sapala, A., and Smith, R. S. (2018). Modeling plant tissue growth and cell division. In Morris, R. J., editor, *Mathematical modelling in plant biology*, pages 107–138. Springer, Cham.
- Mosca, G., Eng, R. C., Adibi, M., Yoshida, S., Lane, B., Bergheim, L., Weber, G., Smith, R. S., and Hay, A. (2024). Growth and tension in explosive fruit. *Current Biology*, 34:1010–1022.
- Moulton, D. E., Oliveri, H., and Goriely, A. (2020). Multiscale integration of environmental stimuli in plant tropism produces complex behaviors. *Proceedings of the National Academy of Sciences*, 117(51):32226–32237.
- Newell, A. C., Shipman, P. D., and Sun, Z. (2008). Phyllotaxis: Cooperation and competition between mechanical and biochemical processes. *Journal of Theoretical Biology*, 251(3):421–439.
- Nonami, H. and Boyer, J. S. (1993). Direct demonstration of a growth-induced water potential gradient. *Plant Physiology*, 102(1):13–19.
- Oliveri, H., Moulton, D. E., Harrington, H. A., and Goriely, A. (2024). Active shape control by plants in dynamic environments. *Physical Review E*, 110(1):014405.
- Oliveri, H., Traas, J., Godin, C., and Ali, O. (2018). Regulation of plant cell wall stiffness by mechanical stress: a mesoscale physical model. *Journal of mathematical biology*, 78(3):625–653.
- Onsager, L. (1931). Reciprocal relations in irreversible processes. I. *Physical review*, 37(4):405.
- Ortega, J. K. E. (1985). Augmented Growth Equation for Cell Wall Expansion. *Plant Physiology*, 79(1):318–320.
- Ortega, J. K. E. (2010). Plant cell growth in tissue. *Plant physiology*, 154(3):1244–1253.
- Passioura, J. B. and Boyer, J. S. (2003). Tissue stresses and resistance to water flow conspire to uncouple the water potential of the epidermis from that of the xylem in elongating plant stems. *Functional Plant Biology*, 30(3):325–334.
- Peng, Z., Alique, D., Xiong, Y., Hu, J., Cao, X., Lü, S., Long, M., Wang, Y., Wabnik, K., and Jiao, Y. (2022). Differential growth dynamics control aerial organ geometry. *Current Biology*, 32(22):4854–4868.
- Peters, W. S. and Tomos, A. D. (1996). The history of tissue tension. *Annals of Botany*, 77(6):657–665.
- Philip, J. (1958). Propagation of turgor and other properties through cell aggregations. *Plant Physiology*, 33(4):271.

- Piecznywek, P. M. and Zdunek, A. (2017). Compression simulations of plant tissue in 3D using a mass-spring system approach and discrete element method. *Soft matter*, 13(40):7318–7331.
- Plant, R. E. (1982). A continuum model for root growth. *Journal of Theoretical Biology*, 98(1):45–59.
- Press, W. H., Teukolsky, S. A., Vetterling, W. T., and Flannery, B. P. (2007). *Numerical recipes: The art of scientific computing*. Cambridge University Press, New York, 3 edition.
- Preziosi, L. and Farina, A. (2002). On Darcy’s law for growing porous media. *International Journal of Non-Linear Mechanics*, 37(3):485–491.
- Rebocho, A. B., Southam, P., Kennaway, J. R., Bangham, J. A., and Coen, E. (2017). Generation of shape complexity through tissue conflict resolution. *eLife*, 6:e20156.
- Robinson, S. and Kuhlemeier, C. (2018). Global compression reorients cortical microtubules in Arabidopsis hypocotyl epidermis and promotes growth. *Current Biology*.
- Rodriguez, E. K., Hoger, A., and McCulloch, A. D. (1994). Stress-dependent finite growth in soft elastic tissues. *Journal of Biomechanics*, 27(4):455–467.
- Rojas, E. R., Hotton, S., and Dumais, J. (2011). Chemically Mediated Mechanical Expansion of the Pollen Tube Cell Wall. *Biophysical Journal*, 101(8):1844–1853.
- Rudge, T. and Haseloff, J. (2005). A computational model of cellular morphogenesis in plants. In *European Conference on Artificial Life*, pages 78–87. Springer.
- Rueda-Contreras, M. D., Romero-Arias, J. R., Aragon, J. L., and Barrio, R. A. (2018). Curvature-driven spatial patterns in growing 3D domains: A mechanochemical model for phyllotaxis. *PLoS One*, 13(8):e0201746.
- Sachs, J. (1865). *Handbuch der Experimental-Physiologie der Pflanzen: Untersuchungen über die allgemeinen Lebensbedingungen der Pflanzen und die Functionen ihrer Organe*, volume 4 of *Handbuch der Experimental-physiologie der Pflanzen*. Wilhelm Engelmann, Leipzig.
- Sachs, J. (1882). *Vorlesungen über Pflanzen-physiologie*, volume 1. W. Engelmann, Leipzig.
- Sassi, M., Ali, O., Boudon, F., Cloarec, G., Abad, U., Cellier, C., Chen, X., Gilles, B., Milani, P., Friml, J., Vernoux, T., Godin, C., Hamant, O., and Traas, J. (2014). An Auxin-Mediated Shift toward Growth Isotropy Promotes Organ Formation at the Shoot Meristem in Arabidopsis. *Current Biology*, 24(19):2335–2342.
- Schopfer, P. (2006). Biomechanics of plant growth. *American journal of botany*, 93(10):1415–1425.
- Tiero, A. and Tomassetti, G. (2016). On morphoelastic rods. *Mathematics and Mechanics of Solids*, 21(8):941–965.

- Vandiver, R. and Goriely, A. (2008). Tissue tension and axial growth of cylindrical structures in plants and elastic tissues. *Europhysics Letters*, 84(5):58004.
- Vandiver, R. and Goriely, A. (2009). Morpho-elastodynamics: the long-time dynamics of elastic growth. *Journal of biological dynamics*, 3(2-3):180–195.
- Wada, H. (2012). Hierarchical helical order in the twisted growth of plant organs. *Physical Review Letters*, 109(12):128104.
- Wang, Q. and Zhao, X. (2015). A three-dimensional phase diagram of growth-induced surface instabilities. *Scientific reports*, 5(1):8887.
- Whitewoods, C. D. and Coen, E. (2017). Growth and development of three-dimensional plant form. *Current Biology*, 27(17):R910–R918.
- Whitewoods, C. D., Gonçalves, B., Cheng, J., Cui, M., Kennaway, R., Lee, K., Bushell, C., Yu, M., Piao, C., and Coen, E. (2020). Evolution of carnivorous traps from planar leaves through simple shifts in gene expression. *Science*, 367(6473):91–96.
- Xue, S.-L., Li, B., Feng, X.-Q., and Gao, H. (2016). Biochemomechanical poroelastic theory of avascular tumor growth. *Journal of the Mechanics and Physics of Solids*, 94:409–432.
- Zhang, H., Xue, F., Guo, L., Cheng, J., Jabbour, F., DuPasquier, P.-E., Xie, Y., Zhang, P., Wu, Y., Duan, X., Kong, H., and Zhang, R. (2024). The mechanism underlying asymmetric bending of lateral petals in *Delphinium* (Ranunculaceae). *Current Biology*, 34:755–768.
- Zhang, Z., Runions, A., Mentink, R. A., Kierzkowski, D., Karady, M., Hashemi, B., Huijser, P., Strauss, S., Gan, X., Ljung, K., and Tsiantis, M. (2020). A WOX/auxin biosynthesis module controls growth to shape leaf form. *Current biology*, 30(24):4857–4868.
- Zhao, F., Du, F., Oliveri, H., Zhou, L., Ali, O., Chen, W., Feng, S., Wang, Q., Lü, S., Long, M., Schneider, R., Sampathkumar, A., Godin, C., Traas, J., and Jiao, Y. (2020). Microtubule-mediated wall anisotropy contributes to leaf blade flattening. *Current Biology*, 30(20):3972–3985.
- Zhu, H. and Melrose, J. (2003). A mechanics model for the compression of plant and vegetative tissues. *Journal of theoretical biology*, 221(1):89–101.